

Instabilities and Insulator-Metal transitions in Half-Doped Manganites induced by Magnetic-Field and Doping

O. Cépas,^{a,b,*} H. R. Krishnamurthy,^{a,c} and T. V. Ramakrishnan^{a,c,d}

a. Department of Physics, Indian Institute of Science, Bangalore 560012, India.

b. Institut Laue Langevin, BP 156, 38042 Grenoble, France.

c. Jawaharlal Nehru Centre for Advanced Scientific Research, Jakkur, Bangalore 560 064, India.

d. Department of Physics, Banaras Hindu University, Varanasi 221005, India.

(Dated: June 6, 2018)

We discuss the phase diagram of the two-orbital model of half-doped manganites by calculating self-consistently the Jahn-Teller (JT) distortion patterns, charge, orbital and magnetic order at zero temperature. We analyse the instabilities of these phases caused by electron or hole doping away from half-doping, or by the application of a magnetic-field. For the CE insulating phase of half-doped manganites, in the intermediate JT coupling regime, we show that there is a competition between canting of spins (which promotes mobile carriers) and polaronic self-trapping of carriers by JT defects. This results in a marked particle-hole asymmetry, with canting winning only on the electron doped side of half-doping. We also show that the CE phase undergoes a first-order transition to a ferromagnetic metallic phase when a magnetic-field is applied, with abrupt changes in the lattice distortion patterns. We discuss the factors that govern the intriguingly small scale of the transition fields. We argue that the ferromagnetic metallic phases involved have two types of charge carriers, localised and band-like, leading to an effective two-fluid model.

I. INTRODUCTION

"Half-doped" manganites, corresponding to the general formula $\text{Re}_{1-x}\text{A}_x\text{MnO}_3$ with $x = 1/2$ where Re is a 3+ rare-earth metal ion and A a 2+ alkaline earth metal ion, eg., $\text{La}_{1/2}\text{Ca}_{1/2}\text{MnO}_3$, have been the object of extensive experimental and theoretical studies for many years.^{1,2} Here each Mn has an average valence of 3.5+ i.e., an average configuration of $d^{3.5}$, corresponding to one $\text{Mn-}e_g$ electron for every two Mn sites hopping around amongst the two $[(x^2 - y^2) \text{ and } (3z^2 - r^2)] e_g$ orbitals on each Mn. The remaining three t_{2g} electrons on each Mn are spin-aligned by strong correlations (Hund's rules) to form "core spins" with $S = 3/2$. Similarly to the end members, i.e., LaMnO_3 or CaMnO_3 , the half-doped compounds, thanks to their commensurate filling, are simpler in some ways than the doped manganites for general x .^{1,2} Nevertheless, they exhibit a very rich variety of properties as well.¹ Specifically, as the system is cooled, there are phase transitions involving changes in magnetic, charge and orbital order, and, in some cases, metallicity. The details vary from material to material, depending systematically on the sizes of the "A site" ions of the perovskite structure. Generally, the lowest temperature phase is insulating, with simultaneous charge, orbital and CE type antiferromagnetic order (see below), and the charge/orbital order sets in first, at higher temperatures, compared to the antiferromagnetic order (e.g., for PrCa $T_{\text{CO/OO}} \sim 240\text{K}$, whereas $T_N \sim 170\text{K}$).³ The NdSr and PrSr systems show ferromagnetic metallic order at intermediate temperatures, but in the LaCa and PrCa systems, the different phases obtained with increasing temperature continue to be insulating. Typically, the charge order and insulating behaviour at low temperatures persist on the "over-doped" side ($x > 1/2$), whereas the charge order disappears rather quickly on the "under-

doped" side ($x < 1/2$), and is often accompanied by metallicity (except in the PrCa system, which stays insulating for all x). This asymmetry between "electron doping" and "hole doping" away from half-doping is a striking feature of the majority of the half-doped manganites.

One simplifying feature of the half-doped manganites is that the low temperature phase is generally regarded as reasonably well characterised. Early neutron diffraction work by Wollan and Koehler⁴ suggested that the magnetic structure of $\text{La}_{1/2}\text{Ca}_{1/2}\text{MnO}_3$ can be viewed as a set of ferromagnetic zig-zag chains antiferromagnetically ordered relative to each other, with an 8-sublattice, $(2\sqrt{2} \times 2\sqrt{2})$ unit cell, and is referred to as the CE magnetic order (Fig. 1). The structure was qualitatively explained soon thereafter by Goodenough,⁵ who proposed additionally that the phase also has a 2-sublattice, $\sqrt{2} \times \sqrt{2}$ charge order with alternating Mn^{3+} and Mn^{4+} sites, and a 4-sublattice, $2\sqrt{2} \times \sqrt{2}$ striped orbital order, as indicated in Fig. 1. Since then, CE order has been found in several other half-doped systems, such as $\text{Nd}_{1/2}\text{Sr}_{1/2}\text{MnO}_3$ ^{6,7} or $\text{Nd}_{1/2}\text{Ca}_{1/2}\text{MnO}_3$ ⁸, though some, such as $\text{Pr}_{1/2}\text{Sr}_{1/2}\text{MnO}_3$,^{6,7} show A-type antiferromagnetism, corresponding to $[0,0,\pi]$ spin order, i.e, ferromagnetic planes of spins which are antiferromagnetically aligned in the z-direction).

The presence of charge and orbital order is, however, harder to establish directly experimentally because of the lack of experimental probes that couple directly to them. Indeed, the perfect $\text{Mn}^{3+}/\text{Mn}^{4+}$ charge ordering proposed by Goodenough⁵ is currently regarded as controversial^{9,10,11,12}. X-ray diffraction data do suggest the presence of large Jahn-Teller (JT) distortions of the oxygen octahedra surrounding the Mn sites^{7,13} with two inequivalent Mn sites, of effective valence $3.5 + \delta$ and $3.5 - \delta$, but δ is not really known, and is unlikely to be

close to 0.5. In $\text{Pr}_{0.6}\text{Ca}_{0.4}\text{MnO}_3$ (which is slightly underdoped though), the charge or valence contrast seems further reduced, and it has been suggested on the basis of neutron diffraction data that the electron is rather shared by two Mn sites paired in dimer-like structures, referred to as "Zener Polarons", with $(\delta \ll 0.5)$.¹⁰ It is not clear, however, whether this is due to the presence of additional electrons¹⁴ or a general feature of many half-doped manganites.¹⁵ A recent work on $\text{Pr}_{0.5}\text{Ca}_{0.5}\text{MnO}_3$ claims indeed to confirm the picture of the original CE state at precisely half-filling.¹⁶ An alternate, closely related picture of the half-doped system is that of a bond-charge-density-wave, with no charge contrast of the Mn ions, substantial hole occupancy on the oxygen ions on the chains, and alternating " O^{2-}/O^- " order.¹⁷ There have been X-ray studies on orbital order and correlations as well as charge and magnetic order using a variety of methods such as soft x-ray resonant diffraction,¹⁸ coherent x-ray scattering,¹⁹ which explore the spatial extent of orbital order, in particular. The resonant scattering experiments in $\text{Pr}_{0.6}\text{Ca}_{0.4}\text{MnO}_3$ conclude that the charge disproportionation is less than complete, that there is orbital mixing, and that therefore the simple Goodenough model is not right. On the other hand, when holes are in excess ($x > 0.5$), it has been suggested that charge order persists but becomes incommensurate.^{20,21}

A closely related family of manganites carefully studied recently is $\text{A}_{0.5}\text{A}'_{0.5}\text{MnO}_3$ where A is a rare earth (Y, Tb, Sm, Nd, Pr, La in order of ion size) and A' is Ba.²² The phases have been studied as a function of A-A' site order/disorder. When there is order, the low temperature phase is charge-ordered (CO) and orbitally ordered (OO) for ion size from Y to Nd. Beyond Nd, up to La, the phase is a ferromagnetic metal. However, when A-A' sites are disordered, there is no CO phase at all, but only a spin glass (SG) phase, from Y to Sm, after which the ground state is ferromagnetic (FM). This means that the CO/FM and CO/SG competition depends on ion size as well on A site ordering in the perovskite ABO_3 structure.

Another interesting and intriguing property of the CE charge-ordered (CE-CO) phase is the magnetic-field-induced insulator-metal transition first discovered in $(\text{Nd,Sm})_{1/2}\text{Sr}_{1/2}\text{MnO}_3$,^{23,24} and later shown to be ubiquitous¹. Though insulating at zero field, these materials become metallic by the application of magnetic-fields of the order of 10 - 40 Tesla via sharp, first-order, resistive transitions.²³ The magnetic-field energies involved are much smaller than the thermal energies (of order 200 K) needed to destroy the charge order, and orders of magnitude smaller than the charge gap of 0.2 - 0.3 eV, as observed as a function of field by STM in $\text{Nd}_{0.5}\text{Sr}_{0.5}\text{MnO}_3$.²⁵ This can be viewed as a different manifestation of the colossal magneto-resistance seen at the metal-insulator transition of doped manganites for $x \sim 0.25$,¹ and the microscopic understanding of the above features poses similar difficult theoretical challenges.^{1,2}

Theory. A variety of models and mechanisms have

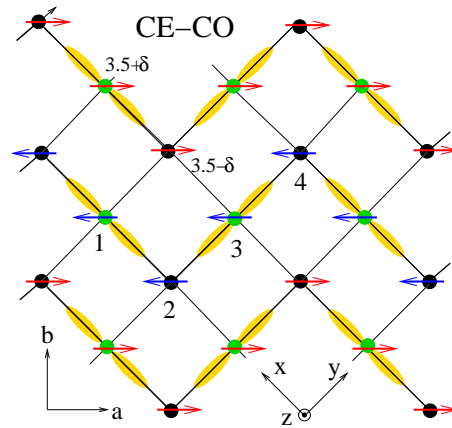


FIG. 1: (color online). A depiction of the CE charge-ordered antiferromagnetic phase (CE-CO). The "bridge sites" (1,3), at the centers of the arms of the zig-zag chains which are ferromagnetically ordered, have alternate occupancies of the $3x^2 - r^2$ and $3y^2 - r^2$ orbitals. At the "corner sites" (2,4), there is no orbital order, unless JT interactions are present. δ is the charge disproportionation between the occupancies of the corner sites and the bridge sites.

been examined in the context of half-doped manganites as well.¹ The simplest model has mobile electrons moving amongst *non-degenerate* orbitals, coupled to the Mn t_{2g} core spins by a large Hund's rule (double) exchange coupling J_H . The latter promotes ferromagnetism, but competes with a direct antiferromagnetic coupling J_{AF} between the core spins. Even in this simple model, the ferromagnetic or CE types of order are stabilised depending upon the strength of J_{AF} .^{26,27} Van den Brink *et al.* considered a more realistic model with the two types of e_g orbitals of Mn, and found that the CE phase is orbitally-ordered: the "bridge sites" of the zig-zag chains have alternating preferred occupancy of $(3x^2 - r^2)$ and $(3y^2 - r^2)$ orbitals²⁸ as indicated in Fig. 1. They also showed that a charge contrast δ (not bigger than 0.2) can be generated by including on-site Coulomb interaction. This is because the "corner sites" turn out to have equal occupancy of $(x^2 - y^2)$ and $(3z^2 - r^2)$ orbitals, and that costs Coulomb energy. To reduce this, the system adopts a preferred occupancy of the bridge sites which are orbitally ordered. In later work, nearest neighbour Coulomb interactions were also included.^{29,30} However, the charge order due to long-range Coulomb interactions is generally of the Wigner-type with wave vector $Q = (\pi, \pi, \pi)$, contrary to the $(\pi, \pi, 0)$ order, with charge stacking along the z-direction, suggested by experiment. To stabilise the $(\pi, \pi, 0)$ order in a wider regime of parameters, JT interactions between the Mn ions and their surrounding oxygen octahedra, which are supposed to be quite large,¹³ have to be included.³¹ The consequent JT distortions further lower the energy of the CE phase because of the already present $(3x^2 - r^2)/(3y^2 - r^2)$ orbital order. Classical Monte Carlo simulations including static JT distortions on small clusters as well as self-

consistent mean field treatments of models including JT and Coulomb interactions³¹ suggest that the CE charge stacked state has the lowest energy in an intermediate range of J_{AF} , unless the nearest neighbour coulomb interaction V becomes much too large.

However, to our knowledge very few of these studies have addressed the other issues, such as the magnetic-field-induced insulator metal transition, and the electron-hole asymmetry. The first issue was tackled in refs. [26,27,32] by assuming model parameters very close to the phase boundary between the ferromagnetic and CE states. The resulting small energy difference between the two phases can then be overcome by an arbitrary small magnetic-field. But it is hard to justify why the system parameters should be so finely tuned for so many systems. As regards the second issue, band structure arguments,²⁸ and treatments including JT distortions on small clusters³¹ necessarily lead to metallic phases upon addition of electrons or holes, in contrast to experiments.

Recently, a theory for doped manganites has been proposed³³ where it is argued that due to strong JT interactions the e_g electrons dynamically reorganise themselves into two types. The majority of the electrons (labelled ℓ) become localised polarons, trapped by large local JT distortions; and a minority of them (labelled b) can remain mobile and non-polaronic. Still virtual adiabatic transitions to empty neighbouring sites induces a ferromagnetic exchange referred as *virtual* double exchange.³³ The resulting Falicov-Kimball like, $\ell - b$ model Hamiltonian treated in a simple dynamical mean-field treatment in the framework of an "orbital liquid" description, gave a good account of the properties of doped manganites.³³

In this paper, we propose an extension of the above theory to the half doped case, which has to include the possibilities for orbital, charge, and antiferromagnetic order. We obtain pointers to this by studying the properties of electronic excitations *coupled with JT defects* in the lattice distortion pattern. We find that such a study suggests the incipient instabilities of the CE phase indicative of the doping and magnetic-field induced phase transitions seen experimentally, as well as the presence of localised and mobile carriers. The localised states on the defects which we obtain are different from the microferions suggested at small x around a dopant,² as they are self-generated and could exist even in the absence of chemical disorder. In principle, the JT defects we are considering could be mobile on a longer time-scale, although disorder may indeed pin them down.

More specifically, in this paper, we first determine the zero temperature phase diagram of the 3d two-orbital model of half-doped manganites for periodic phases in the *thermodynamic limit*, including JT distortions, but ignoring Coulomb interactions. We do this by minimising the energy assuming a periodic unit-cell of eight sites,³⁴ inside which static JT distortions and core spin directions are allowed to be arbitrary. This allows us to determine them self-consistently without using finite-size clusters, thereby extending and reinforcing earlier work.^{31,60} In

particular we obtain analytic results for the phase boundaries at strong JT coupling.

Next, we show that the periodic ferromagnetic phase obtained at small J_{AF} by the method discussed above can become unstable with respect to a phase with two types ($\ell - b$) of electrons when the JT coupling is lowered. We show indeed that it becomes energetically favourable to create single site JT defects, i.e. release the distortion on a finite number of sites that were previously distorted and promote previously trapped electrons onto a mobile band, thus suggesting a metallic phase. The exact nature of the phase can not be figured out by such an instability analysis. Nonetheless, it suggests an effective ($\ell - b$) Hamiltonian with orbital degrees of freedom explicitly included.

The observed phases at half-doping, such as the CE phase, are antiferromagnetic, corresponding to appropriately larger values of J_{AF} . But they show transitions to ferromagnetic metallic phases in an external magnetic-field or when electrons are added. To understand such transitions, in addition to considering changes in the JT distortions, canting of spins is important.

Canted phases are expected to appear not only in a magnetic-field, but also upon doping with carriers (and irrespective of their nature), following the original argument by de Gennes.³⁵ Here we show, however, that canted metallic phases appear only when *electrons* (and not holes) are added, because of the underlying asymmetry of the density of states at half-doping. When we allow for JT distortions, we find a competition with a disordered phase where the added electrons are trapped by JT distortions, the latter phase winning only at small electron concentration. On the hole-doped side, added holes are simply trapped by the lattice distortions and the system remains insulating. Thus our work provides an explanation for the particle-hole asymmetry near $x \sim 1/2$, at intermediate JT couplings which we argue are relevant for the majority of the manganites.

Similarly, we find that there is a strong interplay between turning on a magnetic-field at half doping and the JT distortion pattern. This is consistent with x-ray measurements in $\text{La}_{1/2}\text{Ca}_{1/2}\text{MnO}_3$ in a field.^{38,39} Starting from the distorted CE phase, we find in addition an instability of the high-field ferromagnetic phase to the formation of JT defects. This suggests that the high-field phase seen in experiments may need a two-fluid description.

Interestingly, a very similar two-carrier hypothesis was proposed based on phenomenological grounds to understand the resistivity of $\text{La}_{1-x}\text{Ca}_x\text{MnO}_3$ ($x \sim 1/2$).³⁶ More recently, a particle-hole asymmetric Ginzburg-Landau theory was proposed to explain³⁷ the incommensurate charge order²⁰ seen for $x > 0.5$. We believe that our theory provides the microscopic basis for these facts both.

The rest of this paper is organised as follows. In section II, we discuss the phase diagram of the half-doped manganites restricted to periodic ground states with the

most general 8-sublattice structure. We give in particular an analytic strong-coupling description (IID). In section III, we study the instabilities of some of these phases: instability of the strong JT coupling ferromagnetic phase, which defines a new phase (III A); instability upon doping to the canted phases (III B 1) or to self-trapping of added carriers (III B 2), and the competition between the two (III B 3). The effect of the magnetic-field on the CE phase is studied in section III C, where we also discuss the nature of the high-field ferromagnetic phase. In section IV, we summarise and discuss the possibilities for testing these ideas experimentally. A short account of some of these results has been presented elsewhere.⁴⁰

II. OPTIMISED PERIODIC PHASES AND PHASE DIAGRAM FOR HALF DOPED MANGANITES

A. Model Hamiltonian

Our discussions are based on the following Hamiltonian for the manganites

$$\begin{aligned} \mathcal{H}[\{\mathbf{S}_{ia}, Q_{ia}, \Theta_{ia}\}] = & - \sum_{ij\alpha\beta ab} \tilde{t}_{abij}^{\alpha\beta}(\mathbf{S}_{ia}, \mathbf{S}_{jb}) c_{ia\alpha}^\dagger c_{jb\beta} \\ & + \sum_{\langle ijab \rangle} J_{AF} \mathbf{S}_{ia} \cdot \mathbf{S}_{jb} - g\mu_B \sum_{ia} \mathbf{H} \cdot \mathbf{S}_{ia} \\ & + \frac{1}{2} K \sum_{ia} Q_{ia}^2 - g \sum_{ia\alpha\beta} Q_{ia} \tau_{\alpha\beta}(\Theta_{ia}) c_{ia\alpha}^\dagger c_{ia\beta} \end{aligned} \quad (1)$$

where $c_{ia\alpha}^\dagger$ creates an e_g electron (in a low-energy-projected Wannier orbital with e_g symmetry⁴¹), on the sublattice site a (Mn site) of the unit-cell i in the 3d cubic lattice, and in the orbital state $\alpha = 1, 2$, with $1 \equiv d_{x^2-y^2}, 2 \equiv d_{3z^2-r^2}$. The original lattice is decomposed into eight sublattices, labelled with a .³⁴ There are N sites and $cN = (1-x)N$ electrons (when $x = 1/2$ the number of electrons is denoted $N_0 \equiv N/2$). The first term is the kinetic energy of the electrons. The hopping parameters are taken to be of the usual Anderson-Hasegawa form⁴² which takes care of the Hund's coupling, $J_H \sum_i \mathbf{S}_{ia} \cdot \mathbf{s}_{ia}$ in the limit of large J_H/t , with \mathbf{S}_{ia} , the $S = 3/2$ core spin formed from the Mn t_{2g} electrons being approximated as a classical spin. As a consequence only the electrons with spin projections parallel to the core spins are present, and their hopping amplitudes are functions of the polar angles of the core spins given by:^{42,43}

$$\begin{aligned} \tilde{t}_{abij}^{\alpha\beta}(\mathbf{S}_{ia}, \mathbf{S}_{jb}) = & t_{abij}^{\alpha\beta} \times \\ & \times \left(\cos \frac{\theta_{ia}}{2} \cos \frac{\theta_{jb}}{2} + \sin \frac{\theta_{ia}}{2} \sin \frac{\theta_{jb}}{2} e^{i(\phi_{ia} - \phi_{jb})} \right) \end{aligned} \quad (2)$$

Here $t_{abij}^{\alpha\beta}$ is the usual, anisotropic and symmetry determined, hopping amplitude³¹ between the e_g orbitals

α and β at the two nearest neighbour sites (i, a) and (j, b) respectively, arising from their hybridisation with the $O - p_\sigma$ orbitals (with $4t/3$ being the hopping between $(3z^2 - r^2)$ orbitals in the z -direction)⁴⁴. The second term J_{AF} is the antiferromagnetic coupling of the t_{2g} core spins that comes from standard superexchange processes.⁴⁵ It can be roughly estimated from the Néel temperature of a system with only t_{2g} core spins, such as CaMnO_3 , although the structure of the half-doped system is not exactly the same. The third term is the Zeeman energy where \mathbf{H} is the external magnetic-field. The last two terms include the Jahn-Teller (JT) phonons and their coupling to the e_g electrons. We neglect the $P_{ia}^2/2M_{ia}$ terms since $\hbar\omega_0 \ll t$ (where ω_0 is the typical phonon frequency), but *include their effects heuristically when we argue that JT defects lead to polaron formation*. Q_{ia} and Θ_{ia} are, respectively, the amplitude (measured in units of the typical JT distortions in these materials) and the angle of the JT distortion at the site (i, a) . The coupling matrix is given by:

$$\tau(\Theta) = \begin{pmatrix} \cos \Theta & \sin \Theta \\ \sin \Theta & -\cos \Theta \end{pmatrix} \quad (3)$$

K is the lattice stiffness of a simplified non-cooperative model where distortions on neighbouring sites are not coupled. More detailed and realistic models would include cooperative JT couplings and coupling to breathing modes such as in the lattice model of Ref. [46].

We have neglected the on-site Coulomb interaction, $U \sum_i n_{ia\alpha} n_{ia\bar{\alpha}}$ between different orbital states. Although it is an important interaction in the problem, we can not treat it using the methods used in this paper except in a mean-field approximation. However, it is effectively taken into account when orbital order occurs. We comment on the effects of its inclusion at appropriate places in the paper. When a local JT distortion occurs on a site, the degeneracy of the e_g orbitals is lifted. If only one electron is present, there is a gain by occupying the lowest energy level. If a second electron is added, however, it has to occupy the higher energy level because of the strong Hund's coupling. There is a compensation and the energy gain vanishes. JT distortions therefore suppress double occupancy of sites, mimicking the effect of U . When $g \ll t$, the distortions are small or zero and it is important to explicitly include U , which does play a role. For instance, it induces a charge-ordering in the CE phase,²⁸ just as a finite g/t does.³¹ When $g \gg t$ (see section IID), JT distorted phases appear naturally, and the inclusion of U is not crucial. Similarly, the inclusion of the term $U \sum_i n_{i\uparrow} n_{i\downarrow}$ is unimportant (completely irrelevant when $J_H \rightarrow \infty$) because the large Hund's coupling prevents double occupancy of this type. We have also neglected the longer range coulomb interactions as they are expected to be weak because of the large dielectric constant of the manganites, and we do not consider issues (such as macroscopic phase separation) which are sensitive to their presence.

Note also that regarding the direct coupling of the t_{2g} spins, we restrict ourselves to a pure Heisenberg superexchange coupling. This may not be absolutely accurate for $S = 3/2$ spins. Further couplings, such as single-ion anisotropies, are certainly present in the real materials, but are not of crucial importance for the issues we focus on in this paper. We therefore restrict ourselves to the Hamiltonian of eq. (1).

B. Method

The Hamiltonian of eq. (1) represents mobile electrons coupled to local classical degrees of freedom that act like *annealed disorder*. The probability weight of a particular configuration of the classical variables is given by $\exp[-F_{el}/(k_B T)]$ where F_{el} is the electronic free energy in the presence of that configuration; their distribution thus has to be determined self-consistently. At zero temperature, it is reasonable to assume that the classical degrees of freedom are frozen and have well-defined values. On a finite lattice these can, in principle, be determined as follows. One can diagonalise the Hamiltonian exactly for a given (arbitrary) configuration of lattice distortions (Q_i, Θ_i) and polar angles of the spins θ_i (for simplicity we are ignoring the azimuthal angles of the spins ϕ_i). For each configuration, one can thus find the electronic energy levels, fill up the states up to the Fermi energy, and calculate the total energy. To obtain the ground state of the system, one then needs to minimise this energy with respect to all the possible configurations of classical variables. Such a procedure can be implemented, for example, using a Monte-Carlo technique⁴⁷ for a finite lattice, but becomes a more and more difficult task as the number of lattice sites, and hence the number of variables, increases.

Since our aim is to explore the physics of the experimentally observed CE state, we adopt a simpler approach. We assume a 8-sublattice periodic structure that is compatible with the periodicity of the CE state, which permits us to tackle the problem in a lower dimensional space of the classical variables. [Needless to say, this rules out the possibility of incommensurate (with respect to the assumed eight sublattice structure) or inhomogeneous phases.] We have implemented a simulated annealing routine to minimise the total energy with respect to (essentially all possible) distortions and spin angles on the 8-sublattices. Thus our approach differs from and is complementary to earlier numerical approaches which have considered small clusters and done a full classical Monte-Carlo simulation for the spin and lattice variables.³¹ For us, the only limitation is the number of sublattices, which we fix to be eight; the system size is vastly larger (we are treating the real 3d case), and practically in the thermodynamic limit. [The system size, i.e., the total number of sites, is 8 times the number of periodic repetitions of blocks of 8 sites (the spin and distortions being the same in all the blocks), and we have

done calculations using up to 6912 blocks.] The computational effort of such an approach compared with that of Ref. [31] is, on one hand, much reduced because we do not have to equilibrate a large number of variables. On the other hand, the calculation of the energy of each configuration takes more time because we sum over a large number of k-points (equal to the number of blocks) in the Brillouin zone corresponding to the periodic structure. We have carefully studied the finite-size effects on these Brillouin zone sums. The error on the total energy due to the truncation of the sums is of the order of $10^{-2}t$ where t is the typical energy scale of the problem. The thermodynamic limit is therefore reached within this accuracy, i.e., for all the phases compatible with the sublattice structure we expect that our results are within 1% of the thermodynamic limit results.

C. Results

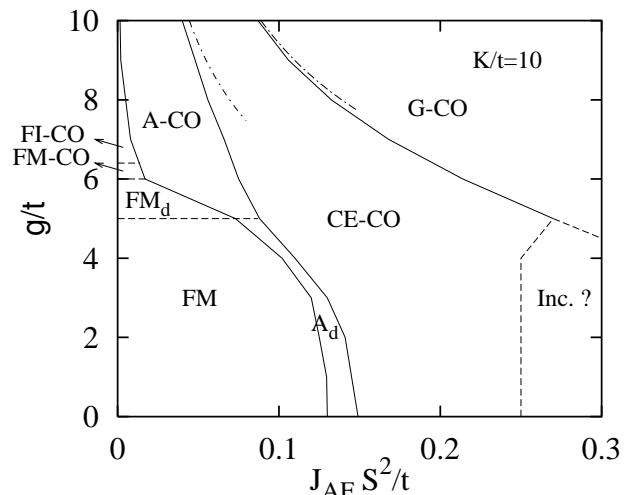


FIG. 2: Phase diagram of the 3D two-orbital model ($T = 0$, $x = 0.5$, $K/t = 10$). FM (resp. FM_d): ferromagnetic metallic phase with no distortions (resp. small uniform distortions). FI-CO (resp. FM-CO): charge-ordered ferromagnetic insulating (resp. metallic) phase with distortions that favour occupancy of the $x^2 - y^2$ orbitals (Fig. 3). A_d: ferromagnetic planes AF aligned with uniform distortions. A-CO: A with charge order. CE-CO: Ferromagnetic zig-zag chains AF ordered, charge and orbital ordered ($3x^2 - r^2/3y^2 - r^2$) [Fig. 1]. G-CO: Néel AF phase with charge-order. Inc.: Possible incommensurate states that interpolate between CE and G. Dotted dashed lines come from analytical expressions derived in the strong-coupling limit (section IID). Solid (dashed) lines show first-order (second-order) phase transitions.

Figure 2 shows the phase diagram as a function of the JT coupling, g/t , and the antiferromagnetic coupling, $J_{AF} S^2/t$, at zero temperature. [We choose units such that the JT distortions are dimensionless, whence K and g both have dimensions of energy, which we spec-

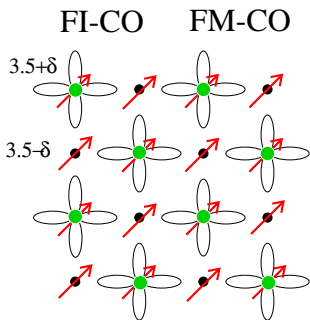


FIG. 3: (color online). A depiction of the ferromagnetic insulating (resp. metallic) charge-ordered phase (FI-CO [resp. FM-CO]) stable at strong JT coupling and small antiferromagnetic coupling (see fig. 2). Alternate sites have charge disproportionation δ (given in Fig. 5 as a function of g/t). The sites with higher occupancies also have strong JT distortions (see fig. 4), of such orientation as to promote the occupancy only of $(x^2 - y^2)$ on these sites, leading to orbital order as well. Note that the lattice is rotated by 45 degrees with respect to fig. 1.

ify in units of t . We use a fixed $K/t = 10$. To compare with earlier work, the JT energy is then $E_{JT}/t = (g/t)^2/(2K/t) = (g/t)^2/20$. We basically find the same phases that were found before either by comparing the energies of selected phases at $g = 0$,^{28,29,48} or by Monte-Carlo simulations at finite g ;³¹ except that now we have provided confirmation that they are indeed the optimal 8-sublattice structures in the thermodynamic limit.

We now describe the different phases shown in Fig. 2, including the amplitudes of the JT distortions in them and the corresponding electronic properties.

For small values of J_{AF} an undistorted metallic phase with 3-d ferromagnetic order (FM) is stable up to a critical value of $g/t \sim 5$. Above this threshold, there is a ferromagnetic phase with very small uniform distortions (Fig. 4), noted FM_d . There is also a narrow region ($5.6 < g/t < 5.9$) where the solution displays many inequivalent sites. As discussed later, we believe that this is consistent with the instability that we find in section III. For $g \gtrsim 5.9$, the stable phase is the FM-CO followed by the FI-CO. These phases have the structure depicted in Fig. 3; i.e., a layered structure with large JT distortions on two sites out of four in a checker-board pattern in each layer, and oriented in such a way as to favour the $(x^2 - y^2)$ orbital on the strongly distorted sites (Fig. 3). There is a charge disproportionation δ that is given in Fig. 5. The structure is metallic (FM-CO) up to $g/t \sim 6.3$, and is insulating (FI-CO) for larger g/t , as is clear from Fig. 6. This structure has been found before,³¹ and is known to compete with a similar structure which prefers a $(3x^2 - r^2)/(3y^2 - r^2)$ orbital order, when strong anharmonic and cooperative JT couplings are taken into account.³²

The A phases, which are more stable at larger J_{AF} (the larger the g/t , the smaller the coupling J_{AF} required for the transition) are similar to the ferromagnetic phases we

have just described except that successive layers are now antiferromagnetically ordered. For g/t up to ~ 5.1 , the phase noted A_d is uniformly distorted with a distortion amplitude given in Fig. 4. It is metallic in this regime (see the charge gap in Fig. 6). For larger values of g/t , the A phase become charge-ordered and insulating, as in case of the FI-CO phase (Fig. 3).

The CE-CO phase, the CE phase with charge stacked order and orbital order (Fig. 1), is the stablest over a wide range of parameters for intermediate J_{AF} , as is clear from (Fig. 2). As pointed out in Refs. [28,31], there is orbital ordering even at $g = 0$, but no charge ordering; the "bridge sites" having an average occupancy of 0.5, but only of $(3x^2 - r^2)$ and $(3y^2 - r^2)$ orbitals alternately (Fig. 1). The "corner sites" on the other hand, have equal occupancy (0.25 each) of $(x^2 - y^2)$ and $(3z^2 - r^2)$ orbitals. The sites are undistorted at $g = 0$, but get distorted as soon as $g > 0$ (Fig. 4, bottom-left panel). The distortions on the bridge sites are the largest, and are oriented in such a way as to further stabilise the alternating occupancy of the $(3x^2 - r^2)$ and $(3y^2 - r^2)$ orbitals that already exists at $g = 0$, since distortions that precisely favour this alternation lower the energy of the system. In addition, small distortions get generated also on the corner sites that favour the $(x^2 - y^2)$ orbital (Fig. 4). As a further consequence, a charge disproportionation δ between the bridge and corner sites develops, favouring a higher occupancy of the former. The variation of δ with g/t is shown in Fig. 5. The system is an insulator whatever the charge disproportionation, as shown by the finite charge gap in Fig. 6.

For strong JT coupling ($g/t \gg 1$), the CE-CO phase is degenerate energetically with the C-CO phase which consists of straight ferromagnetic chains antiferromagnetically ordered with respect to each other. The charge order is accompanied by orbital order of the $(3z^2 - r^2)$ type if the chains are oriented along the z -direction. This degeneracy is discussed in explicit detail in section IID. In this limit, it is easy to show (see section IID) that the G phase (completely 3d-AF phase with localised electrons) is always the stablest for large values of J_{AF} . For smaller values of g/t (and large J_{AF}) we find solutions with many inequivalent (canted) sites, suggesting that the transition from the CE phase to the G phase in this regime might proceed via intermediate states that are incommensurate relative to the periodicity of the unit-cell we have considered (Fig. 2).

We consider next the strong JT coupling limit, $g/t \gg 1$, whence we can calculate the energetics of the phases and the phase boundaries discussed above analytically.

D. Localised description for $g/t \gg 1$

At large g/t , it is energetically favourable for all the electrons in the system to be self-trapped by local lattice distortions since the JT energy gain is large. We hence start with Wannier-type wave-functions with electrons

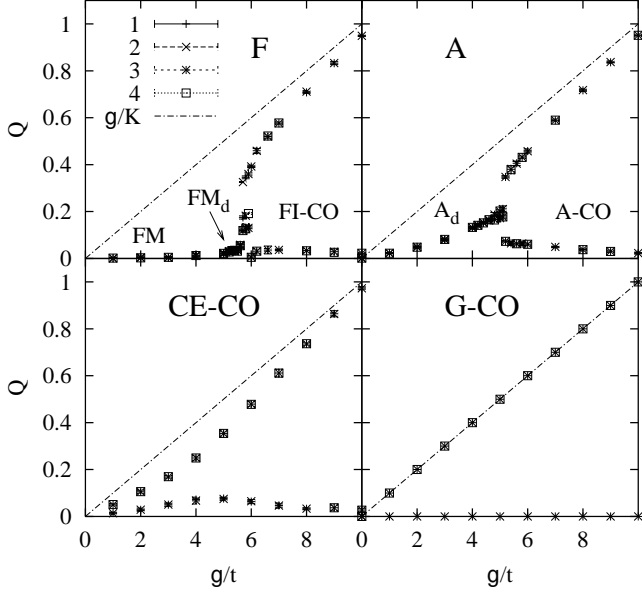


FIG. 4: Amplitudes of distortions of the four inequivalent sites of the unit-cell as function of the coupling parameter g/t . The different panels represent the various phases found previously: F, A, CE, G. The last three phases do not exist for all values of g/t ; the curves are then obtained by fixing the magnetic structure and optimising with respect to the distortions. For the G-CO phase, the distortions are exactly given by g/K since the electrons are completely localised.

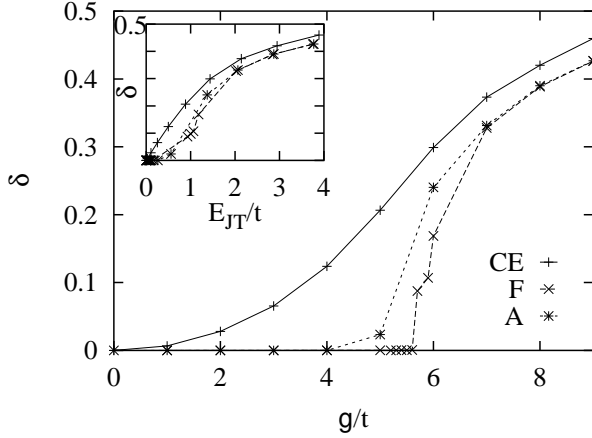


FIG. 5: Charge disproportionation defined by the valence of the two inequivalent Mn ions, $\text{Mn}^{3.5+\delta}$ and $\text{Mn}^{3.5-\delta}$ (see Figs. 1 and 3), as a function of g/t (or E_{JT}/t [inset]) defined by $2E_{JT} = gQ_{max}$, where Q_{max} is the distortion of the site with the largest distortion) for the CE, F and A type-phases.

fully localised on strongly distorted sites. The local energy per electron is the sum of the elastic energy $\frac{1}{2}KQ^2$ and the electronic energy gain $-gQ$ which is minimal at $Q = g/K$ with a net energy gain of $E_{JT} = g^2/(2K)$. In the limit of large g/t , there is a large degeneracy because electrons can be trapped on any site and in any

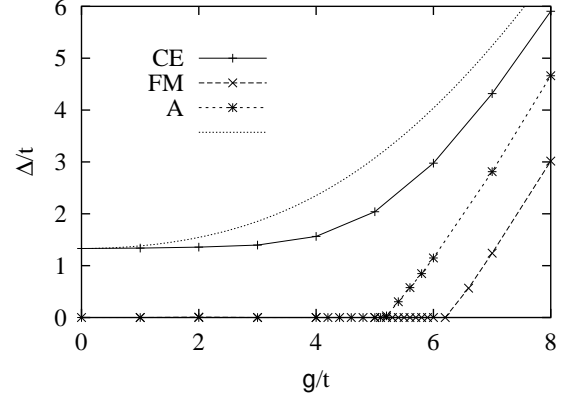


FIG. 6: Charge gap vs. g/t for the CE, F and A type-phases. The CE phase is always insulating, while the A and F phases are insulating beyond $g_{cA}/t = 5.1$, and $g_{cF}/t \sim 6.3$. The dotted line is the gap obtained with non-optimised distortions (eq. (11) in III B).

orbital state, as long as the orbital state correlates with the orientation Θ_i of the JT distortion as

$$|\Psi(\Theta_i)\rangle = \cos \frac{\Theta_i}{2} |d_{x^2-y^2}\rangle + \sin \frac{\Theta_i}{2} |d_{3z^2-r^2}\rangle \quad (4)$$

(for instance, $\Theta_i = -\pi/3$ for $3x^2 - r^2$, and $\Theta_i = \pi/3$ for $3y^2 - r^2$).

This degeneracy is lifted at second-order in perturbation theory in the kinetic energy of the electrons. Consider an electron localised on a site with an empty neighbouring site and with the corresponding core spins aligned. Then, in the adiabatic limit ($t \gg \hbar\omega_0$ where ω_0 is the frequency of the JT phonons) appropriate here, it can hop virtually onto any of the two orbital states of that site and back, without giving the lattice distortions time to relax (the relevant energy denominator being $2E_{JT}$), and hence lower its energy. This energy lowering is less if the core spins are misaligned whence the hopping amplitude is reduced (and even fully suppressed in case of anti-alignment). It is also less if the neighbouring site is occupied, whence the energy denominator is larger, equal to $4E_{JT}$ ($4E_{JT} + U$ in the presence of U , so that the process gets suppressed altogether for large U). Such a process hence gives rise to a effective double exchange term in the Hamiltonian as pointed out in ref. [33] and labelled virtual double exchange. The dominant term in the effective Hamiltonian is then⁴⁹:

$$\tilde{\mathcal{H}} = -E_{JT} \sum_i n_i + \sum_{\langle ij \rangle} J_{AF} \mathbf{S}_i \cdot \mathbf{S}_j - g\mu_B \sum_i \mathbf{H} \cdot \mathbf{S}_i - \frac{J}{2} \sum_{\langle i,j \rangle} (\mathbf{S}_i \cdot \mathbf{S}_j + S^2) [n_i(1-n_j)C_{i,j}^2 + (i \leftrightarrow j)] \quad (5)$$

Here $E_{JT} = g^2/(2K)$, n_i is the electronic occupancy on site i , $J = \tilde{t}^2/(2E_{JT}S^2)$, $\tilde{t} = 4t/3$. $C_{i,j} \equiv$

$\cos[(\Theta_i + \Psi_{ij})/2]$ with $\Psi_{i,i+x} = \Psi_{i+x,i} = +\pi/3$, $\Psi_{i,i+y} = \Psi_{i+y,i} = -\pi/3$ and $\Psi_{i,i+z} = \Psi_{i+z,i} = \pi$.

The effective Hamiltonian of eq. (5) is a *classical* spin-charge-orbital model with no quantum fluctuations. If the charges are assigned specific positions (so as to minimise the energy), the model reduces to a spin-orbital model. It is different from the spin-orbital model proposed for undoped LaMnO_3 obtained by projecting out double occupancies⁵⁰ because double occupancy is irrelevant in the limit being explored here. The orbital (and JT distortion orientation) variables on neighbouring sites are not directly coupled in this model (as C_{ij} involves only one orbital angle Θ_i). Such a coupling would arise if one takes into account a direct coupling between JT distortions on neighbouring sites, as in the cooperative JT model. Nevertheless, even in this simplified approach, the virtual double exchange lifts the degeneracy between different orientations of the JT distortions and the corresponding orbital degeneracy. In addition, it clearly favours ferromagnetic bonds and charge disproportionation.

We can now understand the strong-coupling limit of the phase diagram (Fig. 2), and furthermore even in the presence of a magnetic field, by estimating the energies of the various phases using equation (5). For the fully charge disproportionated phases the energies per site are obtained by minimising \mathcal{H} with respect to the canting angle (at finite fields) and orbital angle (the latter depends on the field for the CE phase, and only the leading term in $H \rightarrow 0$ is given):

$$\begin{aligned} E_{FI-CO} &= 3J_{AF}S^2 - 3JS^2/2 - g\mu_BHS \\ E_{A-CO} &= J_{AF}S^2 - 3JS^2/2 - \frac{(g\mu_BH)^2}{8J_{AF}} \\ E_{C-CO} &= -J_{AF}S^2 - JS^2 - \frac{(g\mu_BH)^2}{16J_{AF} - 2J} \\ E_{CE-CO} &= -J_{AF}S^2 - JS^2 - \frac{(g\mu_BH)^2}{16J_{AF} - J} \quad (H \rightarrow 0) \\ E_{G-CO} &= -3J_{AF}S^2 - \frac{(g\mu_BH)^2}{24J_{AF} - 6J} \end{aligned}$$

At zero field, there is only one free parameter, J_{AF}/J , which determines the relative energies. At $J_{AF} = 0$, the FI phase (which is orbitally disordered in this limit) is degenerate with the A-type phase (with $(x^2 - y^2)$ orbital order), but the latter is favoured as soon as $J_{AF} > 0$. There is a succession of *first-order* phase transitions as J_{AF}/J is increased, first to the CE-CO phase (degenerate with the C-CO phase) at $J_{AF}/J = 1/4$ and then to the G-CO phase (see Fig. 7). In terms of the original variables, the first transition at $1/4$ is located at $J_{AF}S^2/t = 4tK/(9g^2)$; the second transition is at $J_{AF}S^2/t = 8tK/(9g^2)$. The phase boundaries given by these equations in the strong-coupling regime are displayed as dash-dotted lines in the phase diagram (Fig. 2) and are in good agreement with the phase boundaries obtained numerically.

Similarly we can compare the energies of the different phases as a function of the magnetic-field and draw the corresponding phase diagram in the $(J_{AF}/J, g\mu_BH/JS)$ plane (Fig. 7). The degeneracy between the C and the CE phases is lifted and the C phase wins at finite fields. This is because the fourth term of (5) favours Wigner-crystal type of ordering. For the C phase, for instance, the critical field is $g\mu_BH_c = 8J_{AF}S - JS$.

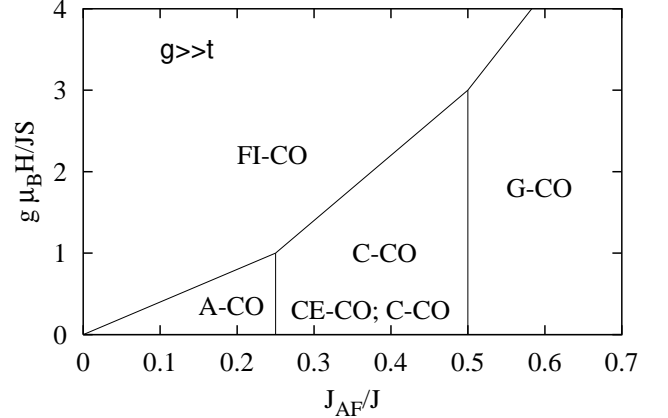


FIG. 7: Phase diagram when $g/t \gg 1$ at $T = 0$ ($x = 0.5$). The phases are the same as in Fig. 2. $JS^2 = \tilde{t}^2/2E_{JT}$. The CE-CO and C-CO phases are degenerate at zero-field, but the latter wins at finite fields.

As noted earlier, in the limit of large g/t much of the physics is insensitive to the inclusion in the model of the on-site Coulomb interaction between different orbital states, $Un_{i\alpha}n_{i\bar{\alpha}}$. The total energy is hardly affected since double occupancy is much reduced. We emphasise again that this is contrary to what happens in the other limit $g/t \ll 1$ where the electron density is uniform. In the latter case, it is known that U by itself will induce charge-ordering in the CE phase,²⁸ at least if the latter is not destabilised by other phases.⁵¹ In the CE phase at large g/t , U will slightly modify the charge contrast by pushing the electrons further off the corner sites. We have performed a self-consistent Hartree-Fock calculation to confirm this point. At $g = 0$, the calculation gives the same results as the slave-boson approach.²⁸ At $g/t = 7$ and for the optimised lattice distortions, the charge contrast increases, with respect to $U = 0$, by a very small amount of order 0.05 for U/t even as large as 25. Therefore, we conclude that the effect of U is small and does not change the nature of the insulating phases in the limit of large g/t .

We next consider the interesting question as to what the appropriate low energy effective Hamiltonian replacing (5) is when t/E_{JT} becomes sufficiently large that perturbation theory in t/E_{JT} and the Hamiltonian (5) are not valid anymore. We argue below, by studying the excitations and instabilities of the original model (1) in the ferromagnetic phase, that the effective model that replaces (5) when t/E_{JT} gets larger takes a similar form

except that mobile electrons have to be included.

III. INSTABILITIES OF THE PERIODIC PHASES

We have discussed in the previous section the various phases stable in the thermodynamic limit that are periodic with a 8-sublattice unit-cell. We will discuss in this section several instabilities that point to non-periodic phases, at half-doping (III A) and also upon doping (III B) or addition of a magnetic-field (III C). We will show that the ferromagnetic insulating phase (FI-CO) is in fact unstable when g/t is lowered below a critical value $g_c/t \sim 6.8$. This instability occurs *before* any of the transitions discussed above (at $g_c/t \sim 6.3$ and 5.9) take place.

For this purpose, we study the energetics of defects in the lattice distortion pattern of the periodic phases. We consider particle and hole excitations *accompanied by single site JT defects*. We consider both types of defects, one where we add a distortion on a site that was previously undistorted, and the other where we remove the distortion of a site that was distorted. Without the lattice distortion defect, the lowest energies of the particle or hole excitations accessible are the appropriate gaps determined by the band-structures discussed in section II C (Fig. 6). The defect modifies locally the JT energy level, and hence constitutes a scattering potential for the particle and hole excitations. The problem lacks lattice translation invariance, and we have solved it by exact numerical diagonalisation of Hamiltonian (1) *represented in real-space*. We consider a problem of N sites (up to $N = 1728$) with one special site, and we calculate all the eigenvalues and the total energy. A key question is whether bound states with energies lower than that allowed by band-structure can appear near the defect. We find that they do in several cases, and when their binding energy exceeds the gap, it signals an instability of the periodic phase.

A. Instability of the Ferromagnetic Insulating Phase when g/t is decreased

We consider first the FI-CO phase at half-doping (pictured in Fig. 3). It is stable for very small J_{AF} and large g/t (see the phase diagram in Fig. 2). Out of the two sites in the unit-cell, one site is distorted with a distortion orientation that favours the $d_{x^2-y^2}$ orbital.

We now consider the problem when one introduces a single site JT defect: the amplitude of the distortion Q of the FI-CO phase is maintained at $N/2 - 1$ sites except at one site where the distortion is now reduced to $Q - Q_d$. Q_d takes all values from 0 (no defect) to Q (the lattice distortion has been completely removed on this site). The excess energy of such a state is given by:

$$E - E_0 = E_{el}(N_0, Q, Q_d) - E_{el}(N_0, Q, 0)$$

$$+ \frac{1}{2}K(Q - Q_d)^2 - \frac{1}{2}KQ^2 \quad (6)$$

Here E_0 and $E_{el}(N_0, Q, 0)$ [$N_0 = N/2$ is the number of electrons] are the total and *electronic* ground state energies of the optimal FI distorted phase, obtained as a function of g/t by minimising with respect to Q as discussed in the previous section. $E_{el}(N_0, Q, Q_d)$ is the *electronic* ground state energy of the defective state. One expects a gain in lattice energy and a loss in electronic energy, because one energy level has been raised at one site. To evaluate the latter, we first solve numerically the problem of the one electron eigenvalues in the presence of the extra single site potential for a finite-size system. Then we calculate $E_{el}(N_0, Q, Q_d)$ by filling the $N/2$ lowest one-electron levels. We have so far considered 3d systems with up to $N = 1728$ sites.

Fig. 8 shows the energy $E - E_0$ plotted vs. Q_d for different values of g/t . We have checked that finite size effects are negligible (the curves corresponding to $N = 216, 1000, 1728$ are given for $g/t = 6.7$ in Fig. 8). For large g/t , the energy is positive but there is a local minimum at large Q_d which can be described as a particle-hole excitation with reduced distortion on one site. When g/t decreases, this excitation softens and vanishes at $g_c/t \sim 6.8$. We believe that this signals the onset of a new phase where such defects are energetically favourable and thus proliferate in the system.

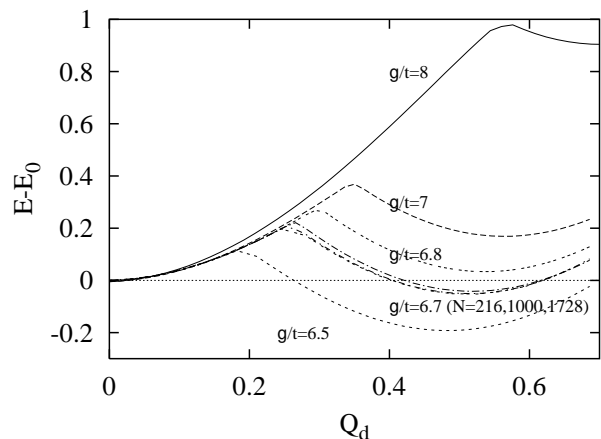


FIG. 8: Energy change when a single JT defect is introduced in the FI-CO phase, vs. Q_d . $Q - Q_d$ is the JT distortion on a defect site; all the other occupied sites having the same distortion Q . We see that there is an excitation with $Q_d \sim Q$ that softens when g/t decreases. The excitation corresponds to a band particle-hole excitation with the removal of a lattice distortion of one site, while the $Q_d = 0$ minimum is the polaron. The softening for $g_c/t \sim 6.8$ signals a phase transition with proliferation of mobile electrons and defects. Finite-size effects are small and shown for $g/t = 6.7$ ($N = 216, 1000, 1728$).

From the calculation of the energy levels in the presence of the defect, we find that there is no bound state within the gap for the Q_d that minimises the energy. The electron occupies a higher-energy band-like state and is

mobile. The instability therefore corresponds to the energy of this mobile electron crossing the chemical potential (i.e., $-E_{JT}$). This suggests that the proliferation of the defects leads to the conversion of some small fraction of the localised electrons into mobile electrons moving on weakly distorted sites, resulting in a metallic phase. Such a state would not be accessible in the minimisation procedure of section II (which has a maximal unit cell of 8 sites) even if the defect sites were to arrange themselves in a super-lattice.

The situation is rather similar to that described by Ramakrishnan *et al.* at the metal-insulator transition in hole doped manganites in the orbital-liquid regime;³³ except that we have here a calculation in the context of a microscopic model that explicitly suggests such a picture even when g/t is not very large. Thus we can identify the high-energy mobile electrons as the *broad-band* b -like electrons of ref. [33], and the low-energy localised states as the ℓ polarons. In the present context, at half-doping and above the transition ($g > g_c$), all the electrons occupy the ℓ states, which form a regular checker-board array (Fig. 3). The sites are singly occupied and U does not play a crucial role. This is no longer the case below the transition when we start to transfer some electrons from the ℓ states to the b states. The b states are delocalised over the empty sites but also visit the sites occupied with ℓ electrons. Double occupancies become inevitable and U has to be taken into account in order to determine accurately the properties of the metallic state. The question of what kind of new metallic state arises for JT couplings just below the instability is clearly interesting. The mobile electrons, for instance, may be able to destroy the orbital and charge order. While a study of such issues is beyond the scope of the present article, the above results suggest that one should add mobile electrons to the strong-coupling Hamiltonian (5), in order to describe metallic phases with possible partial orbital/charge order:

$$\begin{aligned} \tilde{\mathcal{H}} = & -E_{JT} \sum_i n_{\ell i} + \sum_{\langle i,j \rangle} J_{AF} \mathbf{S}_i \cdot \mathbf{S}_j \\ & - \frac{J}{2} \sum_{\langle i,j \rangle} (\mathbf{S}_i \cdot \mathbf{S}_j + S^2) [n_{\ell i}(1 - n_j)C_{i,j}^2 + (i \leftrightarrow j)] \\ & - \sum_{\langle i,j \rangle} t_{ij}^{\alpha\beta} b_{i\alpha}^\dagger b_{j\beta} + \sum_i U n_{i\alpha}^b n_{i\bar{\alpha}}^\ell \end{aligned} \quad (7)$$

where the orbital index α of the mobile b electrons takes both values on the undistorted sites, but is constrained to be orthogonal to the ℓ orbital on the occupied sites, and the other quantities have the same meanings as in eq. (5). For infinite U the mobile electrons can-not hop to the ℓ sites at all, and the last pair of terms can simply be replaced by $-\sum_{\langle i,j \rangle} t_{ij}^{\alpha\beta} b_{i\alpha}^\dagger b_{j\beta}(1 - n_{\ell i})(1 - n_{\ell j})$. This Hamiltonian needs to be studied in a framework that can handle the strong interaction effects, such as the dynamical mean-field theory, in a similar way as was done before for the orbital-liquid state.³³ Note further-

more that the above Hamiltonian does not include $\ell - b$ hybridisation effects, which must be included in order to describe properties sensitive to $\ell - b$ coherence which can develop at sufficiently low temperatures in the metallic phases.³³ It is straightforward to generalise the Hamiltonian to include these effects, as well as cooperative JT effects.

B. Instability of the CE Phase upon Doping

In the band picture of the CE phase^{28,52}, doping with electrons, corresponding to $x < 1/2$ (resp. holes, corresponding to $x > 1/2$) provides mobile carriers in the conduction (resp. valence) band. In either case, the system will be metallic. This is contrary to experiment, where, in most cases, the system remains insulating for $x > 1/2$, but typically becomes metallic quickly for $x < 1/2$. The transition to the ferromagnetic metal for $x < 1/2$ has been described as being due to the crossing of the energies of the CE and ferromagnetic metallic states.²⁸ The transition is then naturally first-order. However, as discussed in ref. [33] even for $x < 1/2$ a simple band picture of the ferromagnetic metallic state is severely limited. Apart from that, the band picture fails to describe the insulating character of the regime $x > 1/2$ and the particle-hole asymmetry around $x = 1/2$. We discuss this issue next.

It was pointed out a long time ago by de Gennes³⁵, in the context of slightly doped LaMnO_3 , that adding carriers to the antiferromagnetic phase of LaMnO_3 may favour canted structures. The qualitative argument is that at small concentration the carriers gain kinetic energy which is linear in the canting angle whereas the loss of magnetic energy is quadratic in the canting angle. By the same token, adding carriers to the CE phase should lead to canting of the core-spins. As such phases interpolate between the CE and FM phases, the transition to ferromagnetism should be naively second-order.

In view of this, we have calculated the energy of homogeneous CE canted phases (defined in Fig. 9) for different carrier concentrations on either side of $x = 1/2$ (i.e., retaining the 8-sublattice periodic structure even when $x \neq 1/2$). We find that canting is favourable for adding electrons to the half-doped system but not for adding holes, as de Gennes's general argument is valid only for very small carrier concentration and breaks down quickly on the hole side, due to special features of the CE state. We have calculated, in addition, the energy in the presence of a single-site defect in the JT distortion as in the previous subsection. We find that, when g/t is sizeable, canting is in competition with self-trapping of the carriers in JT defects. We find that the energy gain due to trapping is linear in the carrier concentration (and thus dominates at low concentration) whereas it is quadratic for the canting. For intermediate values of g/t , this results in a first-order transition to a canted metallic phase when electrons are added to the half-doped system (i.e., for $x < 1/2$), and the persistence of a CE-type phase

with self-trapped carriers when holes are added (i.e., for $x > 1/2$).

1. Canted Phases

We first consider the total energy of a homogeneous canted CE phase as a function of the canting angle ϕ (see Fig. 9 for definition) for different values of doping (Fig. 10, top). We take the JT distortions that optimise the energy (as discussed in section II), except that we neglect the small distortions on the corner sites for simplicity.⁵³ When adding electrons ($x < 0.5$), the energy of the system is lowered by a finite canting angle (Fig. 10, top). The higher the concentration the higher the canting angle. When adding holes ($x > 0.5$), however, it turns out that the system prefers $\phi = 0$.

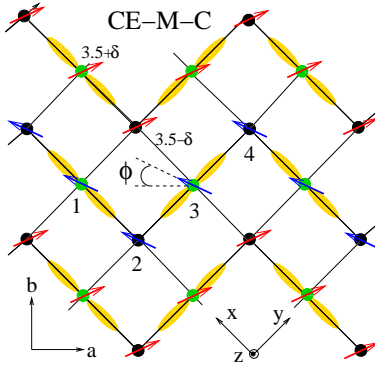


FIG. 9: (color online). Canted CE phase with canting angle ϕ (CE-M-C). The electrons can now hop from chain to chain. The original 1d zig-zag chains are marked with thicker lines.

We can understand these results by considering in more detail the band structure of the CE phase.^{28,52,54} As discussed earlier for $x = 1/2$ (section II), the bridge sites are orbitally ordered in the $(3x^2 - r^2)/(3y^2 - r^2)$ pattern.²⁸ If the Jahn-Teller distortions occur in such a way as to favour precisely the alternation of $(3x^2 - r^2)/(3y^2 - r^2)$ orbitals, the energy of the system is further lowered. The band structure has four dispersive bands and four non-dispersive bands (two at zero and two at finite energy), as shown in Fig. 11 (see Refs. [28,52,54]) and described by:

$$\epsilon_{qa1}^{\pm} = -E_{JT} \pm \sqrt{E_{JT}^2 + \tilde{t}^2(2 + \cos q_a)} \quad (8)$$

$$\epsilon_{qa2}^{\pm} = -E_{JT} \pm \sqrt{E_{JT}^2 + \tilde{t}^2(2 - \cos q_a)} \quad (9)$$

$$\epsilon_{3,4} = 0, \quad \epsilon_{5,6} = 2E_{JT} \quad (10)$$

where $\tilde{t} = 4t/3$ and $E_{JT} = gQ/2$, and the wave-vector q_a , which takes values in the reduced Brillouin zone $[-\pi/2, \pi/2]$, is parallel to the chain direction. The band structure is analogous to that of Ref. [28,52] with a charge ordering coming from the Jahn-Teller distortions,

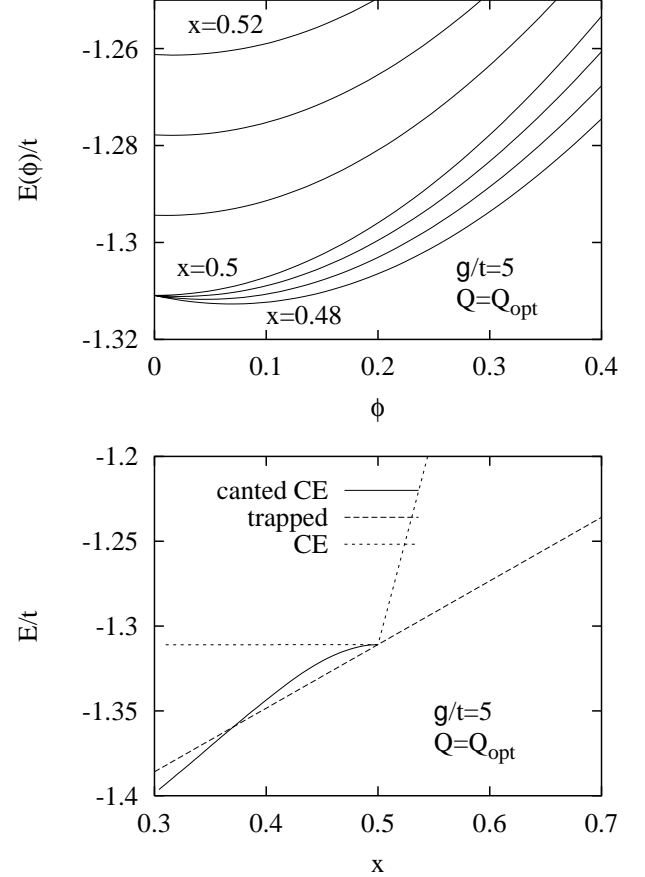


FIG. 10: Top. Energies of the canted phases as function of the canting angle, for different concentrations ($g/t = 5$ and $Q = Q_{opt} = 0.35$). For $x < 0.5$, there is a finite angle that minimises the energy. For $x > 0.5$, the angle is zero and the CE state is stable. Bottom: Comparison of the energies of the different phases. The canting angle is chosen such as to minimise the energy as in the top figure.

as in Ref. [54], but determined self-consistently. At $x = 1/2$, the lowest band is completely filled.

The zero energy band is made up entirely of the states from the corner sites (see appendix A). The charge gap, from the top of the filled valence bands to the zero energy states, is given by:

$$\Delta = E_{JT} + \sqrt{E_{JT}^2 + \tilde{t}^2} \quad (11)$$

When the core spins are canted away from $\phi = 0$, the degeneracy of the zero energy states of the zig-zag chains is lifted, and they form bands which disperse. *To first order in the canting angle*, the dispersion arises from the coupling of the $(3z^2 - r^2)$ orbitals at the corner sites along the z -direction, and is given by:

$$\epsilon^0(q_a, q_z) = -4t\phi \frac{1 + \cos q_a}{2 + \cos q_a} \cos q_z \quad (12)$$

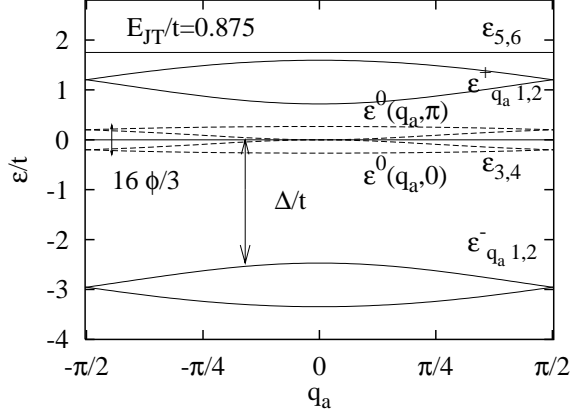


FIG. 11: Band structure of the 1d zig-zag chains (solid lines) with Jahn-Teller distortions ($E_{JT}/t = 0.875$), given by eqs. (8), (9) and (10).^{28,52,54} At $x = 1/2$, only the lowest band is filled. Also shown is the splitting of the zero-energy states (dashed lines) when the core spins are tilted away by an angle ϕ (whence their dispersion becomes 2-dimensional).

Added electrons (with respect to the reference state $x = 1/2$) occupy the bottom of this new band (properly folded in the reduced Brillouin zone, Fig. 11) at $q, q_z \sim 0$. Each electron therefore gains an energy $-\beta_e \phi t$ with $\beta_e = 8/3$, which is completely independent of g . On the other hand, there is an energy loss $\kappa \phi^2$ per site, where κ is the effective spin stiffness towards canting. There are two contributions to κ . One comes from the direct superexchange. In the CE phase with $\phi = 0$, two of the neighbour spins are parallel and the other four neighbour spins are antiparallel. This gives a contribution $4J_{AF}S^2\phi^2$ to the energy. There is also a contribution from the double exchange, which we calculate numerically by calculating the change in the total kinetic energy as function of ϕ . From this we extract a stiffness in the limit of small ϕ , $-\kappa_e = f(g/t, \delta c)$ where $\delta c \equiv 1/2 - x$ is the filling fraction in excess of that at half-doping, so that $\kappa = 4J_{AF}S^2 - \kappa_e$.

The canting angle is then given by minimising the excess energy per site, $E - E_0 = \kappa \phi^2 - \beta_e t \delta c \phi$, and is given by $\phi = \beta_e t \delta c / 2\kappa$. Note that the linear dependence in δc is valid only for sufficiently small δc whence the additional electrons occupy states near the bottom of the band. There are in fact $N/8$ states with energy smaller than 0 and $N/8$ states with energy greater. So the linear dependence is expected to be reasonable for $\delta c \ll 1/8$. The total minimised excess energy is then

$$E - E_0 = -\frac{\beta_e^2 t^2}{4\kappa} (\delta c)^2, \quad (13)$$

quadratic in the electron concentration (E_0 is the energy of the CE phase at $x = 1/2$). The canted CE phase thus has a lower energy than that of the CE phase by this amount, whenever $\delta c > 0$. This explains the quadratic behaviour in δc found numerically in the previous para-

graph (Fig. 10, bottom). When δc increases further, the canting angle increases until eventually the system becomes fully ferromagnetic via a second-order phase transition. Within the above picture, as soon as $\delta c > 0$, the system is metallic because the additional electrons occupy the dispersing conduction band. But note that, since the dispersion is mainly along the z and the chain directions to leading order in the canting angle, the metallicity generated by such a mechanism would be highly anisotropic.

Surprisingly, the situation turns out very differently when excess holes are added to the half-doped system. Naively, one might have thought that canting the spins will push up the states at the top of the lower band and that the added holes will thus gain energy, similarly to the case of electrons. But according to the numerical results of Fig. 10, this is not what happens. The energy is minimal at $\phi = 0$, i.e. when the spins are *not* canted. The reason is that the energy gain for the whole system is not linear in the number of additional holes, except for extremely small δc . This is even more emphatically and dramatically evident from Fig. 12, which shows that the energy gained by canting for a small fixed canting angle ($\phi = 0.05$) as a function of doping, is extremely particle-hole asymmetric. While the gain is indeed linear in the deviation from half doping on either side for the smallest values of $|\delta c|$, it drops quickly and substantially below this, and stays small for $x > 1/2$, i.e., for added holes. In contrast, when electrons are added, the energy gain from canting remains large for large $|\delta x|$. (We emphasise that the above results are only for the canted CE state for any x ; hence they are most meaningful near $x = 1/2$.)

The reason for this asymmetry is the difference in the dispersion of the electron and hole bands in the canted CE phase. As discussed in detail above, the conduction band in the canted CE phase (into which electrons get added) disperses only in two directions, and hence the corresponding density of states is constant, over a bandwidth of order $t\phi$. Hence the energy gain from canting remains substantial up to half occupancy of the conduction band, corresponding to $\delta c = 0.25$, beyond which the energy gain starts reducing because of cancellations, as is clear from Fig. 12 (dashed line). In contrast, the valence band in the canted CE phase which accommodates the holes (and which we have not discussed in detail), disperses in all three directions, resulting in a density of states which starts from zero at the top of the band. Typically when the change in the chemical potential is smaller than $t\phi$, the additional holes occupy the higher energy states of the new band and the energy gain is linear in the number of additional carriers. On the other hand, when the chemical potential is of order $t\phi$, both sides of the new band are occupied and there is no energy gain. The condition is expressed as $\delta c < t\phi\rho(\epsilon_F)$ where $\rho(\epsilon_F)$ is the density of states at the Fermi energy for the system with the concentration $c + \delta c$. When the density of states is small, the range within which the energy gain is linear in the number of carriers is small. In

this range and out of it, the canting angle is then very small because it does not scale with the number of carriers anymore, as is confirmed by Fig. 12.

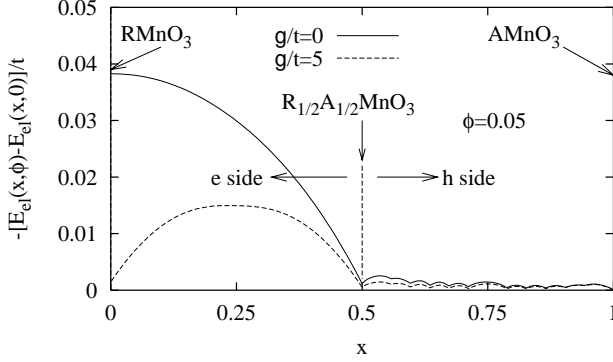


FIG. 12: Energy gained by canting of the CE phase for a fixed canting angle of $\phi = 0.05$ as a function of doping away from half doping, showing the particle-hole asymmetry.

2. Trapping of Added Carriers in the CE Phase

Trapping of Added Electrons: We next explore the competition between the above process and the possible trapping of the added electrons in lattice distortions by allowing for an additional lattice distortion on one special site and $N_0 + 1$ electrons ($N_0 = N/2$). In other words we look at the cost or gain of energy involved in trapping one additional electron in the CE state. Since the added electron goes into a band made up from states belonging to the corner sites which is originally undistorted, we choose the special site with the added distortion to be one of the corner sites, and of such an orientation as to lower the energy of the $(3z^2 - r^2)$ orbital (Fig. 13). As in III A, translation invariance is now broken, and we find the one-electron energy eigenvalues by diagonalizing exactly the problem on large lattices, as a function of the strength of the additional distortion, Q_d . We show the energy levels in Fig. 13, left. In addition to the band states (black areas), we also find a couple of bound-states within the gap (Fig. 13, left).

The total excess energy including the cost of elastic energy to create such a defect in the lattice is calculated by filling up the energy levels with $N_0 + 1$ electrons:

$$E - E_0 = E_{el}(N_0 + 1, Q_d) - E_{el}(N_0 + 1, 0) + \frac{1}{2} K Q_d^2 \quad (14)$$

The energy can be viewed as the sum of three different contributions, each of which is separately shown in Fig. 13: there is the electronic energy gain for the electron bound to the defect, the scattering energy for the electrons that are scattered by the defect (both of which are contained in $E_{el}(N_0 + 1, Q_d)$) and the elastic energy cost for creating such a distortion. When all are put together,

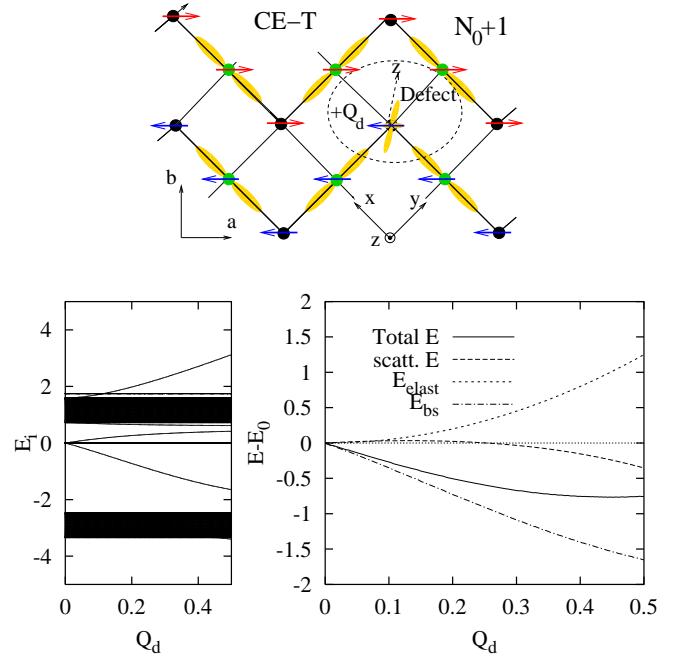


FIG. 13: (color online). Definition of the defect (top), that is an additional distortion of strength Q_d on a single corner site ($(3z^2 - r^2)$ orbital). Energy levels vs. Q_d (bottom left). At $Q_d = 0$, there is no defect and the band structure is that of Fig. 11. At $Q_d > 0$, bound states appear within the gap. Total excess energy of the system with $N_0 + 1$ electrons (bottom right). This can be seen as the sum of the energy of the bound state E_{bs} , the elastic energy E_{elast} and defines the scattering energy E_{scatt} . $g/t = 5$, $Q = Q_{opt} = 0.35$ ($E_{JT} = 0.875$).

it turns out that it is favourable to create a defect with an energy gain, \tilde{E}_{JT}^e . For instance, in Fig. 13, when $g/t = 5$, the energy gain is $\tilde{E}_{JT}^e = 0.75t \sim 0.86E_{JT}$, slightly smaller than E_{JT} due to band structure effects. The problem can not, indeed, be reduced to polaron formation purely with the states of the conduction band by ignoring the valence band (that would give $\tilde{E}_{JT}^e = E_{JT}$). The scattering of electrons by the defect and the level repulsion between the two bands (Fig. 13) accounts for the reduced value of \tilde{E}_{JT}^e found above.

For a small concentration of additional electrons, δc , the energy gain with respect to the CE phase, given by

$$E - E_0 = -\tilde{E}_{JT}^e \delta c, \quad (15)$$

is linear with the concentration of additional electrons. Here E_0 is the energy of the perfect CE phase with additional electrons occupying the (undistorted) zero-energy band states.

When we compare eq. (15) and eq. (13), it is clear that the linear dependence (15) gains over the quadratic dependence (13) of the canted phases at small doping. At small doping then, the system is insulating and the additional carriers are trapped in inhomogeneous lattice distortions. The resulting phase is interesting in that it pos-

sesses some self-induced disorder. Random self-trapping of additional carriers has also been reported in the adiabatic spinless Holstein model, with a concentration of carriers close to one electron for two sites,⁵⁵ that is similar to the present case. By including the double exchange, we have shown that such doping-induced inhomogeneous states are in fact quite general and more stable than the canted states because of the linear energy gain we have found at small concentration. It has some similarities with the inhomogeneous states with metallic droplets found in a simple model with charge-ordering near half-filling.⁵⁶ We note that we have considered here the simplest polaronic state with fully localised electrons on the defect sites. It would be interesting to study whether more complex defects, involving for instance distortions of the magnetic structure on the neighbouring sites (magnetic polaron) could arise near $x \sim 1/2$, as suggested for $x \sim 0$ (ref. [2]) or $x \sim 1$ (ref. [57]).

Trapping of Added Holes: Similarly, it is also favourable to trap added holes in lattice distortions. We consider the analogue of the previous problem with one-less distortion and $N_0 - 1$ electrons. The removal of the distortion on one site creates again a defect. The energy levels and the excess energy calculated numerically by filling the energy levels with $N_0 - 1$ electrons,

$$E - E_0 = E_{el}(N_0 - 1, Q, Q_d) - E_{el}(N_0 - 1, Q, 0) + \frac{1}{2}K(Q - Q_d)^2 - \frac{1}{2}KQ^2 \quad (16)$$

are given in Fig. 14. We find that it is favourable to trap the additional hole onto the bound state that appears within the gap just above the lowest band (Fig. 14, left) as soon as $g/t \gtrsim 4$. The energy gain, \tilde{E}_{JT}^h is smaller than E_{JT} and is $0.31t \sim 0.35E_{JT}$ for $g/t = 5$ (Fig. 14). For the whole system the energy gain is $-\tilde{E}_{JT}^h \delta c$. It is then favourable to trap the holes and the system is insulating.

3. Competition between the two phases and Phase Diagram

By comparing the energies of the canted state and the defective state, (for instance, as shown for $g/t = 5$ in Fig.10) we can arrive at a phase diagram in $g/t - x$ plane near half doping. As discussed above, when electrons are added to the CE phase, they are trapped on corner sites with newly generated Jahn-Teller distortions if their concentration is within $[1/2 - \delta c_{crit}, 1/2]$ (Fig. 15). These JT distortions are oriented in the z -direction, so as to favour the occupancy of the $(3z^2 - r^2)$ orbital. The magnetic structure remains of CE type. For $x = 1/2 - \delta c_{crit}$ there is a transition to a metallic state with canted spins. In the present approach there is a finite canting angle at the transition, so that the transition is first-order. When the concentration increases further the canting angle becomes larger and larger. At small g/t we find that there is a first-order transition line between a canted state with

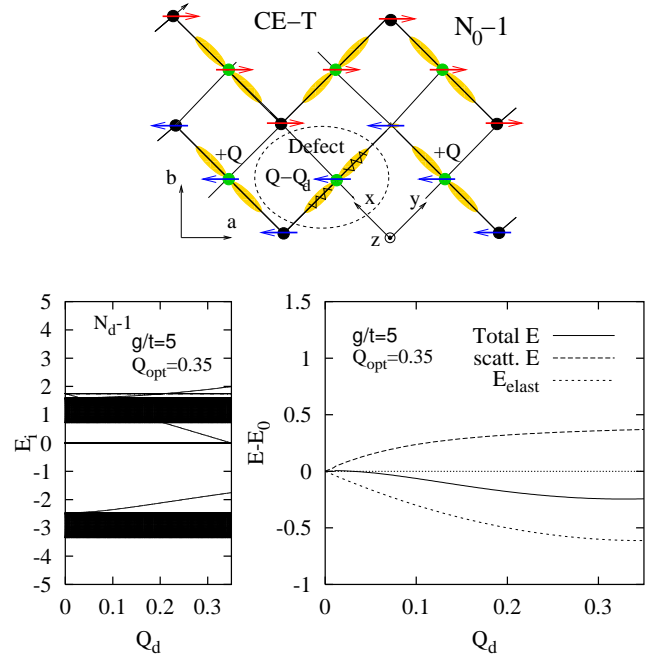


FIG. 14: (color online). Definition of the defect on a single bridge site with distortion decreased to $Q - Q_d$ ($Q_d = 0$ corresponds to a fully distorted site as in the original structure). Energy levels vs. Q_d (bottom left) and energies for $N_0 - 1$ electrons (bottom right). $g/t = 5$.

small canting angle and a highly canted state that ends by a critical point (Fig. 15). The system becomes eventually fully ferromagnetic.

On the other hand, when holes are added to the CE phase, the holes get trapped on bridge sites with lattice distortions removed when $g/t \gtrsim 4$ (and the system remains insulating, CE-T) or move freely in the lowest band for $g/t \lesssim 4$ (and the system is metallic, CE-M) [Fig. 15]. There is no competition with canted states in this case because, as discussed in III B 1, the density of states near the top of the valence band is not large enough to provide sizeable energy gains.

We emphasise that this phase diagram is based on an instability calculation, and can be expected to be accurate only when x is sufficiently close to $x = 1/2$. Away from it, the defects start to interact and other phases may appear.^{12,20,21}

We note that in all our discussions so far we have neglected the disorder that is present in the real systems. In fact, even at half-doping the arrangement of the A site ions (La or Ca) is disordered. This disorder causes the localisation of the one electron states (near the band-edges in 3-d) leading to increased stabilisation of the insulating properties near half-doping, and may also have consequences on the local magnetic structure as emphasised by the idea of ferrons.²

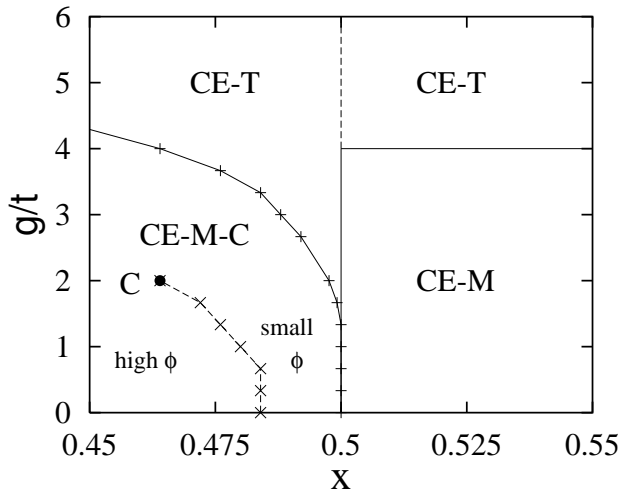


FIG. 15: Phase diagram as a function of the model parameter g/t for hole doping concentration x close to $1/2$ ($J_{AF}S^2/t = 0.15$). CE-M-C denotes a metallic and canted CE phase. CE-T refers to the CE phase with added carriers self-trapped in JT defects.⁵⁸ CE-M is the CE phase with added holes that is metallic (no canting nor trapping of the holes). C is a critical point ending a first-order transition line between two CE-M-C states with differing canting angles that arise for small g/t .

C. Instability of the CE Phase in a Magnetic-Field

Finally, in this subsection we discuss the instabilities of the CE phase in a magnetic-field due to the combined effects of canting of spins towards the direction of the field by a canting angle ϕ (as pictured in Fig. 9) and modification of the JT distortions.

Since a band opens out of the zero energy states upon canting (dashed lines in Fig. 11), the system will "melt" into a metallic phase when the corresponding charge gap closes. Since this can happen for a canting angle less than $\pi/2$, the transition will typically not be to the fully polarised ferromagnetic state.

In Fig. 16, we show the energy versus the canting angle for different fields at $g/t = 0$. There is a small optimal canting angle that minimises the energy for small fields, but the system continues to be insulating. When the field increases further there is a first-order transition to a state with a finite (and large) canting angle, which is metallic. This is reminiscent of the first-order transition line between two canted states when additional electrons are added (section III B and Fig. 15). We note that the first-order transition field is very small, $g\mu_B H_c = 0.010t$, not only because, with $J_{AF}S^2 = 0.15t$ the system is close to the phase boundary, but also because the canted phases reduce the critical field considerably. Previous works that have assumed that the insulator-metal transitions involve the fully ferromagnetic state^{26,27,32} would predict a transition field $g\mu_B H_c = 0.14t$ for the same J_{AF} we have used above. We discuss in detail next as to how these features change with respect to turning on g (and keeping the

same J_{AF}).

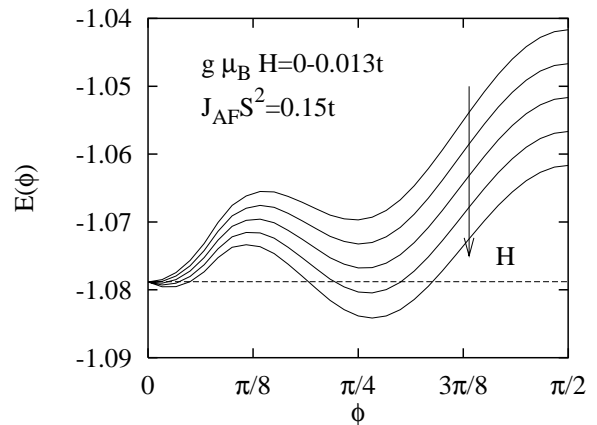


FIG. 16: First-order transition of the CE phase to a canted state when an external magnetic-field is applied to the system at $g = 0$. The threshold field that induces the first-order transition is given by $g\mu_B H_c = 0.010t$. The system is metallic beyond H_c .

1. $g/t \lesssim 5$

To start with we take the CE phase with the optimal lattice distortions found in section II for different values of g/t . First, we *freeze the distortions* for all magnetic-fields and find the optimal canting angle that minimises the energy as a function of the magnetic-field, for non-zero values of g/t (Fig. 17). The jumps in the canting angle correspond to first-order transitions between states with small and large canting angles. When g/t is increased, the transition fields and the fields at which the fully ferromagnetic state is reached shift rather quickly to larger values. The transition field becomes larger simply because, with increasing g/t (and for the same J_{AF}), the system moves further and further away from the phase boundary with the ferromagnetic phase (see the phase boundary in Fig. 2).

We next show that the threshold fields for the "melting" of the CE phase are reduced by taking into account the effect of the magnetic-field on the lattice distortions themselves. One should expect this, since in section II it was shown that the ferromagnetic phases remains undistorted up to $g/t = 5$. It is made explicit in Fig. 18, where the energy of the *undistorted* highly-canted state (solid line), which merge into the fully ferromagnetic state (dashed line) at higher fields, crosses that of the *distorted* canted CE states. These transitions occur at smaller transition fields (see Fig. 18) compared with the transition fields we considered in the previous paragraph (the latter correspond to the cusps, visible in the curves $g/t = 2, 3$ in Fig. 18). The new magnetisation curves are shown in Fig. 19, top. We then calculate the band structure as a function of the magnetic field and extract

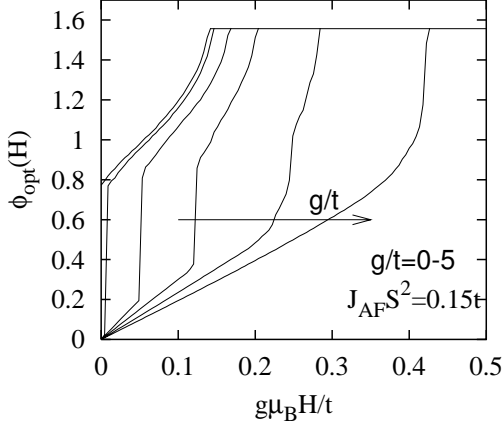


FIG. 17: Optimal canting angle vs. external magnetic-field for different values of g/t (from 0 up to 5) keeping the same distortions as at $H = 0$ (CE phase) for all magnetic-fields. There are first-order transitions between canted states. As we will show, there are other transitions, involving modified JT distortions, that preempt those shown in this figure (see below, Fig. 19).

the gap (Fig. 19, bottom). The jumps in the magnetisation and in the gaps turn out to be simultaneous, thus indicating that the transitions correspond to insulator-metal transitions. The transition fields $g\mu_B H_c$ vary in the range $0.01t - 0.2t$ for $J_{AF}S^2 = 0.15t$. The smaller the g/t the smaller the transition field at fixed J_{AF} .

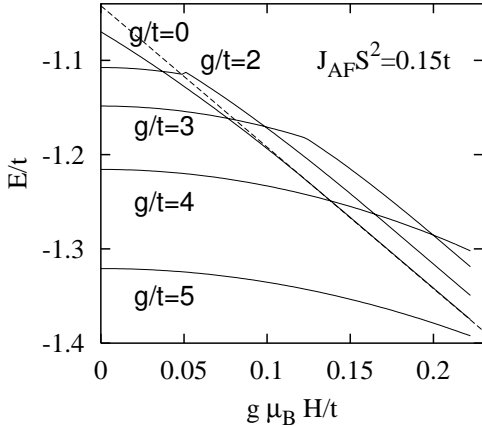


FIG. 18: Crossing of the energies of the *distorted* canted CE phases (solid lines, with $g/t = 2, 3, 4, 5$) with that of the *undistorted* highly-canted phase (solid line corresponding to $g/t = 0$), or the fully ferromagnetic phase (dashed line) to which it merges for large fields. The cusps visible in the $g/t = 2, 3$ curves at higher fields correspond to the first-order transitions described in Fig. 17. But these are preempted by the transitions to the undistorted phase.

The first-order transitions discussed above were obtained by considering the crossing of two solutions, namely the *distorted* canted CE phase (with the distor-

tions frozen at their $H = 0$ values) and the *undistorted* FM phase. It is possible, in principle, that intermediate phases with intermediate distortions appear. To rule out this possibility, we have performed the full optimisation in presence of the external magnetic-field for $g/t = 4, 5$ and found that the decrease in the distortions is less than 6% up to the transition to the undistorted ferromagnetic phase. This validates our approximation of using frozen distortions in the canted CE phase up to the first-order transition.

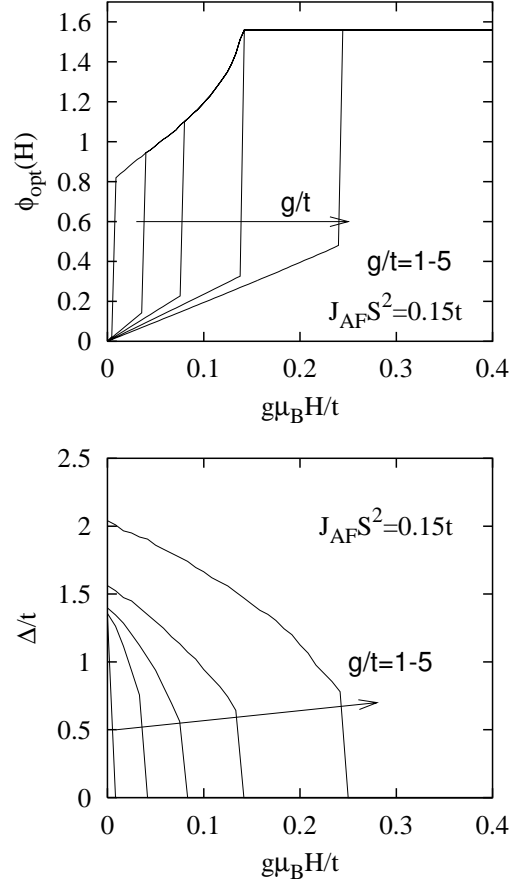


FIG. 19: Magnetisation or canting angle (top) and charge gap (bottom) vs. external magnetic-field for different values of $g/t = 1 - 5$ ($J_{AF}S^2/t = 0.15$). There are clear first-order transitions to an *undistorted* canted metallic or fully ferromagnetic metallic phase.

We can roughly understand some of the above results in terms of an expansion of the physical quantities in the canting angle, before the first-order transition takes place. For simplicity we neglect the distortions on the corner sites of the CE state, so that the zero-energy states are degenerate to start with. The degeneracy is then lifted by the canting and the reduced charge gap is given at first order in the canting angle by:

$$\Delta(\phi) = \Delta - \beta_e t \phi \quad (17)$$

where Δ is the gap of the uncanted CE phase, given

by equation (11), and $\beta_e = 8/3$ a numerical coefficient (from eq. 12). The canting angle itself is determined by minimising the magnetic energy per spin due to canting, given for small ϕ by:

$$E = \kappa\phi^2 - g\mu_B SH\phi \quad (18)$$

where $\kappa \equiv 4J_{AF}S^2 - \kappa_e$ is the spin stiffness we have referred to before (section III B). The energy is minimal for $\phi_{opt}(H) = g\mu_B SH/2\kappa$, which describes the linear regime of the curves in Fig. 19, before the first-order transitions to the highly canted states take place. The corresponding charge gap, given by

$$\Delta_{min} \equiv \Delta(\phi_{opt}) = \Delta - \left(\frac{\beta_e t}{2\kappa}\right) g\mu_B SH, \quad (19)$$

also decreases linearly with field, but is not a very good approximation to the results of Fig. 19, bottom. The difference comes from the small distortions on the corner sites which we neglected in deriving (17) by assuming degenerate zero-energy states. With small distortions on the corner sites, the zero-energy states are no longer degenerate, and that would modify the expression for the gap (17).

In any case, one can give an *upper bound* for the critical magnetic-field by extrapolating the linear expression (19) to zero. This is an upper bound because the actual transition occurs before the gap get completely closed as is clear from Fig. 19. We have

$$g\mu_B SH_c = \frac{2\kappa\Delta}{\beta_e t} = (8J_{AF}S^2 - 2\kappa_e) \frac{\Delta}{\beta_e t} \quad (20)$$

It is clear from this expression that in order to close a gap Δ of order E_{JT} or t , we do not need a magnetic-field of order Δ thanks to the reducing factor κ/t . κ/t is small, first because the spins are easy to polarise on energy scales that have nothing to do with the charge scales, as in the standard field-induced insulator-metal transition of a spin-density wave. It is interesting to note that the large field $g\mu_B SH_{c0} \equiv 8J_{AF}S^2$ is the critical field to align anti-ferromagnetic spins coupled only by J_{AF} . The real transition fields are substantially reduced compared to this by the double exchange included in κ_e and the factor $\Delta/\beta_e t$ which describes how fast the gap closes with the canting angle. For example, the strength of the transitions fields of Fig. 19 are in the range $g\mu_B H_c \sim 0.1t - 0.25t$. With $t \sim 0.2$ eV, we have $g\mu_B H_c \sim 20 - 50$ meV, or $H_c \sim 140 - 350$ Tesla, which are still much too large. We discuss this discrepancy below. We now consider the other situation with $g/t \gtrsim 5.0$.

2. Transition to an Inhomogeneous State

For $g/t > 6.8$ we have seen that even the ferromagnetic phases are insulating. Hence it is to be expected that no insulator-metal transition can take place in this

regime. Instead, the CE phase makes a transition to the ferromagnetic insulating phase for sufficiently large fields, as is clear from the large g/t limit phase diagram discussed in section II D. For $g/t < 6.8$, however, we have shown earlier that it is favourable to create defects and mobile electrons out of the FI-CO phase (section III A). We expect therefore that similar kinds of phases will be favoured by a magnetic-field as well. We explore this issue further below, taking $g/t = 6$ as an example.

We first compare the energy of the canted distorted CE phase [with the usual $(3x^2 - r^2)/(3y^2 - r^2)$ orbital ordering] with that of a canted phase with alternate sites distorted in such a way as to favour the $(x^2 - y^2)$ orbital ordering. The latter is indeed a lower energy state for large g/t when the spins are fully aligned, compared with the undistorted phase. We see in the inset of Fig. 20 that the two energies cross for $g\mu_B H/t \sim 0.43$. As shown in Fig. 20, at this field the canting angle that minimises the energy jumps from ~ 0.8 to $\pi/2$ corresponding to a transition to the fully ferromagnetic state (which is metallic at $g/t = 6.0$, see Fig. 6) with $(x^2 - y^2)$ orbital ordering.

We now consider the possibility of creating a defect in the lattice distortion pattern, similarly to what we discussed in section III A, which might lead to a lower energy according to what we found there. We start with the $(x^2 - y^2)$ phase with canting angle ϕ , and reduce the distortion of one of the distorted sites to $Q - Q_d$ instead of Q , so that when $Q_d = Q$, the distortion is completely removed. In Fig. 21, we show the total energy $E - E_0$ (where E_0 is the energy of the homogeneous phase, corresponding to $Q_d = 0$) as function of Q_d for different canting angles near the transition. Clearly, there is a minimum at $Q_d = Q$ ($Q = 0.39$ at $g/t = 6.0$) that corresponds to an excitation where we remove a distortion and create a particle-hole excitation. This minimum becomes soft at $\phi \sim 0.9$, thus signalling the onset of a transition to a phase where such defects are energetically favourable. Note that this phase can not correspond to the undistorted phase (i.e., to removing the distortions on all the sites) because the undistorted canted phase is higher in energy as is clear from Fig. 20 (short-dashed lines).

To sum up the discussion above, when a magnetic-field is switched on, the core spins cant towards the direction of the field. A band opens out of the zero-energy states of the corner sites of the CE phase and the gap gets reduced. At a threshold value of the magnetic-field, there is an instability toward transferring electrons from the localised states (or lower energy band) to the mobile states. For field values close to this threshold, further energy gain is possible when some Jahn-Teller distortions are removed and defects are created. When the density increases, the missing distortions start to play a more important role and the one-defect approach we have developed here breaks down. This scenario for the magnetic-field induced metallic phase is very close to the description of the metallic phase in the $(x < 0.5)$ regime as discussed in Ref. [33].

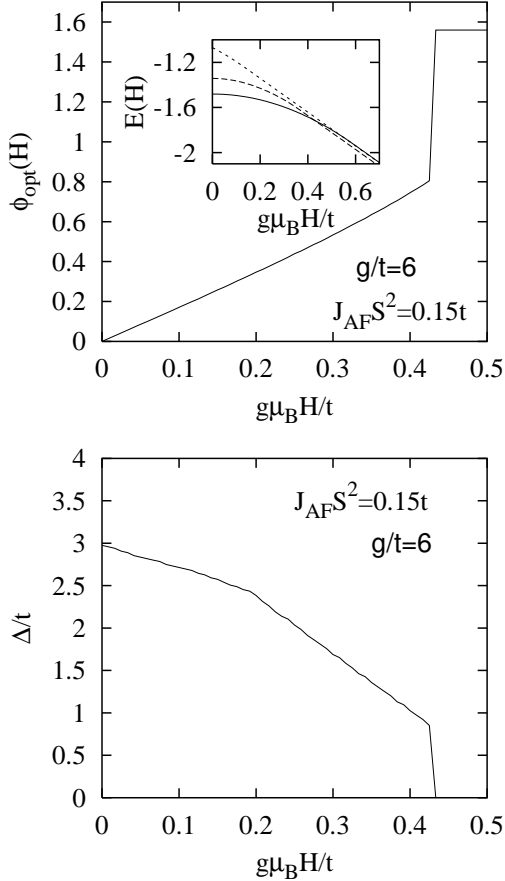


FIG. 20: Magnetisation or canting angle (top) vs. external magnetic-field for $g/t = 6$ ($J_{\text{AF}}S^2/t = 0.15$). In the inset the energies of the undistorted canted phase (dotted line), the canted phase with distortions so as to favour $(x^2 - y^2)$ orbital ordering (dashed line) and the CE canted phase (solid line) are given. The latter two cross for $g\mu_B H/t$ around 0.43, where the first-order transition takes place. Above this field the phase is fully ferromagnetic. Bottom: The resulting Charge Gap is shown as a function of $g\mu_B H/t$

Clearly, for all the values of g/t we have considered, there are rich transitions from the CE phase to the ferromagnetic phases as a function of the magnetic-field. The lattice distortions play a crucial role in converting a transition that would be naturally second-order because of the progressive canting of the spins into a first-order transition.

The strength of the magnetic-field at which the transition occurs, although much reduced compared to naive estimates as discussed above, is still much too large compared to experiment, especially if we consider large values of g/t . However, the large distortions observed experimentally are consistent with relatively large values of g/t . How does one reconcile these two? As we have seen, a crucial ingredient that determines the strength of the transition field is the charge gap. We can reasonably argue that the gap is overestimated in the present ap-

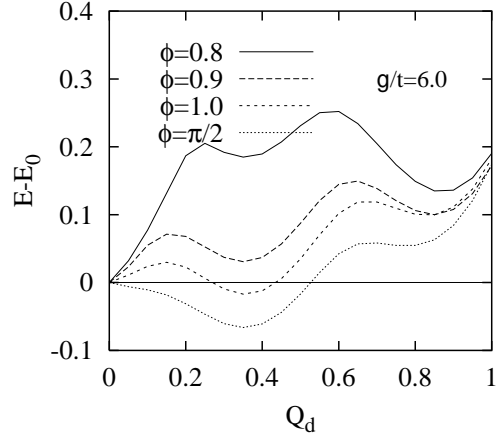


FIG. 21: Energy for creating a single-site defect in the JT distortions with amplitude Q_d for various canting angles in the FI phase. Such an excitation becomes soft at $\phi = 0.95$ and the defects proliferate. The transition corresponds to an instability towards a metallic phase with defects.

proach. On the experimental side, the gap is not of the order of t but much smaller, typically 5 times smaller for $\text{Nd}_{1/2}\text{Ca}_{1/2}\text{MnO}_3$.⁵⁹ This is also clear from the temperature at which the charge-order transition takes place. If we use the estimates of the gap from experiments in the expression (20), the transition field comes out to be much smaller, of order 30 T, much closer to the transition fields of that compound.

It is clearly important, therefore, to improve the theory presented above to generate a more accurate estimate for the charge gap in the CE phase. For this we need to include at least three sources of correction to the gap estimate above. Namely the finiteness of the Hund's coupling J_H , the cooperative nature of the JT distortions, and small second neighbour hoppings. When J_H is finite, the electrons can hop even between sites which have anti-aligned core spins. This opens a band out of the zero energy states and reduces the gap. Second, because distortions of neighbouring sites are coupled, a distortion on a site imposes a distortion on the neighbouring site that lowers the energy level, thereby reducing the gap. Finally, second neighbour hopping allows the corner site electrons to become mobile (even in the case of infinite J_H), and overall increases the bandwidths of all the bands, hence reducing the charge gap (see, for example, ref. [54]). We believe that, while the theory presented above clarifies how the smallness of the transition field arises, a more elaborate theory including these three effects which reduce the gap is required to obtain a precise estimate of the transition field.

IV. CONCLUDING REMARKS

In conclusion, we have first confirmed various periodic phases of the phase diagram of half-doped manganites

(Fig. 2), by optimising the lattice and magnetic energies in the thermodynamic limit. We have thus provided explicit calculations for the Jahn-Teller distortions, charge and orbital order-parameters in the various stable phases by exploring the phase space in an unbiased way, albeit limited by the 8-site unit-cell.

It is interesting to discuss, in the context of the phase diagram of Fig. 2, the strengths of the couplings of real manganites materials. Obviously, the absence of 3d ferromagnetic phases at half-doping suggests that J_{AF} is substantial in these materials ($J_{AF}S^2/t \gtrsim 0.05$). The observation of the A-type phase in $\text{Pr}_{1/2}\text{Sr}_{1/2}\text{MnO}_3$ with distortions that favour the $(x^2 - y^2)$ orbital,^{6,7} is only compatible with $g/t \gtrsim 5.0$ (Fig. 2), a large value that is generally corroborated by large distortions.¹³ In addition, the fact that many half-doped manganites show a (CE) insulator to (ferro) metal transition as a function of magnetic-field confirms that g/t can not be much larger (since for $g/t \gtrsim 6.3$, the ferromagnetic phase is also insulating). Adopting such values $g/t \sim 5$ (or $E_{JT} \sim t$), the charge disproportionation in the CE phase is $\delta \sim 0.2$ (Fig. 5), which is much smaller than Goodenough's ionic picture value of 0.5. The inclusion of cooperative JT effects is likely to reduce the charge contrast. In addition, the specific distribution of the charge contrast amongst the Mn and O orbitals depends upon band-structure details which we have not considered in this paper.⁴¹

Secondly, and more importantly, we have studied the instabilities of these phases with respect to canting of spins *and* single site defects in their JT distortion pattern, caused by doping away from $x = 0.5$ or by the application of a magnetic-field. The consideration of canted CE phases allowed us to study how the magnetisation changes with applied field. We have found that the distortions do not change much in the linear regime of the magnetisation up to a threshold field at which there is an abrupt change. This seems to be consistent with recent experiments.^{38,39} A more detailed comparison would be interesting in order to extract the strength of the JT coupling. Regarding the effect of the doping, we have found that when electrons are added (with respect to half-doping, i.e., for $x < 0.5$) the transition from an insulating CE phase with self-trapped carriers to the ferromagnetic metallic phase of the colossal magneto-resistance materials proceeds via a first-order transition to canted states. In contrast, added holes (corresponding to $x > 0.5$), do not favour canted states because of a lack of density of states near the top of the valence band. The holes prefer to be self-trapped, at least above a threshold g/t . This, we believe, is the underlying cause of why the most manganites tend to remain insulating and favour incommensurate charge order^{20,21} for $x > 0.5$, but quickly become metallic for $x < 0.5$. This striking particle-hole asymmetry has been recently explored within a Ginzburg-Landau framework³⁷; we believe that our work clarifies the microscopic basis for this asymmetry.⁶¹

We emphasise that the actual numbers we have obtained, such as the threshold g/t and magnetic-field val-

ues for the various transitions may not correspond to experimental data because the model we have studied neglects several important effects such as the cooperative nature of the JT distortions, the finiteness of the Hund's coupling, presence of second neighbour hopping, etc. As pointed out in the previous section, for example, the size of the charge gap in the CE phase, which in turn determines the threshold field for its transition to the ferromagnetic metallic phase, will be reduced when these effects are taken into account.

Finally, and most importantly, in the intermediate JT coupling regime which we have argued is the most appropriate for manganites, we have shown that there is an instability of the ferromagnetic phase to formation of defects in the JT distortion pattern. We did this by calculating the energy cost for creating a single site defect in the lattice distortion; i.e. reducing (and eventually removing) the distortion at that site and promoting a quasi-localised electron onto a mobile band. We have shown that there are parameter regimes where this appears spontaneously. A proliferation of such defects leads to a scenario for the ferromagnetic metallic state that is completely consistent with, and provides a new justification for, the effective two-fluid (one light and extended, the other polaronic and localised) picture proposed recently to explain the insulator-metal transition in the colossal magneto-resistance materials.³³

On the basis of this identification we have suggested a new effective Hamiltonian given by eq. (7) which goes beyond that of Ref. [33] in that it allows for possible orbital and charge ordering effects. We believe that a treatment of this Hamiltonian using more sophisticated methods, such as the dynamical mean field theory,⁶² will eventually lead to a more complete theory of the manganites, including orbital and charge ordering effects. We hope to discuss such work elsewhere.

Nevertheless, our work suggests that the ferromagnetic metallic phase obtained at large magnetic-fields in half-doped manganites is similar to the ferro-metallic phases found upon hole doping, i.e., for $x < 0.5$, except, perhaps for some remanent orbital and charge order. It is an obvious and interesting question as to whether any vestige of the orbital and charge order present in the CE phase survives metallisation. If it does, the metallic phase would also be rather anisotropic, with larger mobility along the z-axis of the CE phase. But irrespective of this, it should have a large fraction of sites which continue to be JT distorted accounting for the majority of the e_g electrons, which remain localised, and only a small number of mobile carriers. Interestingly, this resembles the phenomenological picture of ref. 36. Our results provide a microscopic justification for this picture and can be further tested experimentally in a variety of other ways, such as measurement of Drude weights in optical conductivity, EXAFS and neutron diffraction experiments, for instance.

Acknowledgments

O.C. would like to thank G. Bouzerar, T. Chatterji, G. Jackeli, D. Khomskii, Y. Motome, H. Nojiri and T. Ziman for stimulating discussions. O.C acknowledges financial supports from the I.L.L. and from the Indo-French grant IFCPAR/2404.1.

APPENDIX A: WAVE-FUNCTIONS OF THE CE STATE WITH LATTICE DISTORTIONS

The unit-cell of the 1d zig-zag chains has four inequivalent sites and there are two orbitals per site (see Fig. 1). We list below the eight states, which extends Refs. [28,29,52] to the presence of lattice distortions on the bridge sites. The corresponding energies are given in Fig. 11 and in equations (8) - (10).

$$\begin{aligned}
 (i) \quad \Psi_{q_a,1}^{\pm} &= \frac{A_{q_a,1}^{\pm}}{\sqrt{2}} [|1, 3x^2 - r^2\rangle_{q_a} - e^{iq_a} |3, 3y^2 - r^2\rangle_{q_a}] \\
 &- A_{q_a,1}^{\pm} \frac{2\sqrt{2}t}{3\epsilon_{q_a,1}^{\pm}} [|2, 3x^2 - r^2\rangle_{q_a} + e^{iq_a} |2, 3y^2 - r^2\rangle_{q_a}] \\
 &- A_{q_a,1}^{\pm} \frac{2\sqrt{2}t}{3\epsilon_{q_a,1}^{\pm}} e^{iq_a} [|4, 3y^2 - r^2\rangle_{q_a} + e^{iq_a} |4, 3x^2 - r^2\rangle_{q_a}] \\
 \epsilon_{q_a,1}^{\pm} &= -E_{JT} \pm \sqrt{E_{JT}^2 + \tilde{t}^2(2 + \cos q_a)} \\
 A_{q_a,1}^{\pm} &= \left[1 + \frac{\tilde{t}^2(2 + \cos q_a)}{(\epsilon_{q_a,1}^{\pm})^2} \right]^{-1/2}
 \end{aligned}$$

$$\begin{aligned}
 (ii) \quad \Psi_{q_a,2}^{\pm} &= \frac{A_{q_a,2}^{\pm}}{\sqrt{2}} [|1, 3x^2 - r^2\rangle_{q_a} + e^{iq_a} |3, 3y^2 - r^2\rangle_{q_a}] \\
 &- A_{q_a,2}^{\pm} \frac{2\sqrt{2}t}{3\epsilon_{q_a,1}^{\pm}} [|2, 3x^2 - r^2\rangle_{q_a} - e^{iq_a} |2, 3y^2 - r^2\rangle_{q_a}] \\
 &- A_{q_a,2}^{\pm} \frac{2\sqrt{2}t}{3\epsilon_{q_a,1}^{\pm}} e^{iq_a} [-|4, 3y^2 - r^2\rangle_{q_a} + e^{iq_a} |4, 3x^2 - r^2\rangle_{q_a}]
 \end{aligned}$$

$$\begin{aligned}
 \epsilon_{q_a,2}^{\pm} &= -E_{JT} \pm \sqrt{E_{JT}^2 + \tilde{t}^2(2 - \cos q_a)} \\
 A_{q_a,2}^{\pm} &= \left[1 + \frac{\tilde{t}^2(2 - \cos q_a)}{(\epsilon_{q_a,2}^{\pm})^2} \right]^{-1/2}
 \end{aligned}$$

$$\begin{aligned}
 (iii) \quad \Psi_{q_a,3} &= \frac{A_{q_a,3}}{\sqrt{2}} [|2, y^2 - z^2\rangle_{q_a} + e^{-iq_a} |2, x^2 - z^2\rangle_{q_a}] \\
 &- (2 \rightarrow 4, q_a \rightarrow -q_a) \\
 \Psi_{q_a,4} &= \frac{A_{q_a,4}}{\sqrt{2}} [|2, y^2 - z^2\rangle_{q_a} - e^{-iq_a} |2, x^2 - z^2\rangle_{q_a}] \\
 &- (2 \rightarrow 4, q_a \rightarrow -q_a) \\
 A_{q_a,3} &= (2 - \cos q_a)^{-1/2}; \quad A_{q_a,4} = (2 + \cos q_a)^{-1/2} \\
 \epsilon_{3,4} &= 0
 \end{aligned}$$

$$\begin{aligned}
 (iv) \quad \Psi_{q_a,5} &= |1, y^2 - z^2\rangle_{q_a} \\
 \Psi_{q_a,6} &= |3, x^2 - z^2\rangle_{q_a} \\
 \epsilon_{5,6} &= 2E_{JT}
 \end{aligned}$$

where the notations are $\tilde{t} = 4t/3$, $E_{JT} = gQ/2$ and the states are defined by:

$$|a, \alpha\rangle_{q_a} = \frac{1}{\sqrt{N}} \sum_i e^{iq_a R_i} |i, a, \alpha\rangle$$

with $a = 1, \dots, 4$ the four inequivalent sites of the zig-zag chain and α can be any of the orbital states defined in eq. (4). q_a is the component of the wave-vector along the chain direction. It takes values in the first Brillouin zone $[-\pi/2, \pi/2]$. As for $g = 0$, the degeneracies at $\pm\pi/2$ come from the translation symmetry combined with a mirror plane symmetry. Similarly, the properties $\Psi_{q_a,1}^{\pm} = \Psi_{q_a+\pi,2}^{\pm}$ and $\Psi_{q_a,3} = \Psi_{q_a+\pi,4}$ are consequences of the same symmetry.

* permanent address : Laboratoire de physique théorique de la matière condensée, Université Pierre et Marie Curie, UMR 7600 of CNRS, 4 Place Jussieu, 75252 Paris cedex 5.

¹ e.g., see A. P. Ramirez, J. Phys.: Condens. Matter **9**, 8171 (1997); C. N. R. Rao, and B. Raveau, Eds., *Colossal Magnetoresistance, Charge Ordering and Related Properties of Manganese Oxides* (World Scientific, Singapore, 1998); Y. Tokura, ed. *Colossal Magnetoresistance Oxides* (Gordon and Breach, New York, 2000); C. N. R. Rao, A. Arulraj, A K Cheetham and B. Raveau, J. Phys.: Condens. Matter **12** R83 (2000); M. B. Salamon and M. Jaime, Rev. Mod. Phys. **73**, 583 (2001); E. Dagotto, T. Hotta and A. Moreo, *Physics Reports*. **344**, 1 (2001).

² See also the review by V. N. Loktev and Yu. G. Pogorelov, Low Temp. Physics **26**, 171 (2000) which discusses the ex-

tension to doped manganites of early ideas on the motion of holes in (antiferro) magnetic lattices, and the idea of 'ferions' developed by Nagaev and collaborators mostly in the context of diluted magnetic semiconductors (see e.g. E L Nagaev, Physics of Magnetic Semiconductors Mir, Moscow (1983), and E. L. Nagaev, Usp. Fiz. Nauk **166**, 833 (1996)) including the notions of 'microferions'.

³ C. Martin, A. Maignan, M. Hervieu, and B. Raveau, Phys. Rev. B **60**, 12191 (1999).

⁴ E. O. Wollan and W. C. Koehler, Phys. Rev. **100**, 545 (1955).

⁵ J. B. Goodenough, Phys. Rev. **100**, 564 (1955).

⁶ H. Kawano, R. Kajimoto, H. Yoshizawa, Y. Tomioka, H. Kuwahara, and Y. Tokura, Phys. Rev. Lett. **78**, 4253 (1997).

- ⁷ H. Kawano-Furukawa, R. Kajimoto, H. Yoshizawa, Y. Tomioka, H. Kuwahara, and Y. Tokura, *Phys. Rev. B* **67**, 174422 (2003).
- ⁸ F. Millange, S. de Brion, and G. Chouteau, *Phys. Rev. B* **62**, 5619 (2000).
- ⁹ J. Garcia, M. C. Sanchez, G. Subias, and J. Blasco, *J. Phys. Condens. Matter* **13**, 3229, 3243 (2001).
- ¹⁰ A. Daoud-Aladine, J. Rodríguez-Carvajal, L. Pinsard-Gaudart, M. T. Fernández-Díaz, and A. Revcolevschi, *Phys. Rev. Lett.* **89**, 097205 (2002).
- ¹¹ M. Coey, *Nature* **430**, 155 (2004).
- ¹² D. V. Efremov, J. van den Brink, and D. I. Khomskii, *Nature Materials* **3**, 853 (2004).
- ¹³ P. G. Radaelli, D. E. Cox, M. Marezio, S. W. Cheong, *Phys. Rev. B* **55**, 3015 (1997).
- ¹⁴ e.g., in Ref. 12, it is shown that a similar phase, although not identical as far as the magnetic structure is concerned, has a lower energy when electrons are added to the CE phase. The CE phase is, however, still preferred at half-doping.
- ¹⁵ A. Daoud-Aladine, J. Rodríguez-Carvajal, L. Pinsard-Gaudart, and A. Revcolevschi, *J. Magn. Magn. Mater.* **272**, e1387 (2004).
- ¹⁶ R. J. Goff, and J. P. Attfield, *Phys. Rev. B* **70**, 140404(R) (2004).
- ¹⁷ G. Zheng and C. H. Patterson, *Phys. Rev. B* **67**, 220404(R) (2003); V. Ferrari, M. Towler, and P. B. Littlewood, *Phys. Rev. Lett.* **91**, 227202 (2003); see also Ref. 12.
- ¹⁸ K. J. Thomas, J. P. Hill, S. Grenier, Y.-J. Kim, P. Abbamonte, L. Venema, A. Rusydi, Y. Tomioka, Y. Tokura, D. F. McMorrow, G. Sawatzky, and M. van Veenendaal, *Phys. Rev. Lett.* **92**, 237204 (2004).
- ¹⁹ C. S. Nelson, J. P. Hill, Doon Gibbs, F. Yakhov, F. Livet, Y. Tomioka, T. Kimura, and Y. Tokura, *Phys. Rev. B* **66**, 134412 (2002).
- ²⁰ S. Mori, C. H. Chen, and S.-W. Cheong, *Nature (London)* **392**, 473 (1998); J. C. Loudon, S. Cox, A. J. Williams, J. P. Attfield, P. B. Littlewood, P. A. Midgley, and N. D. Mathur, *Phys. Rev. Lett.* **94**, 097202 (2005).
- ²¹ L. Brey, *Phys. Rev. Lett.* **92**, 127202 (2004).
- ²² See N. Furukawa and Y. Motome, *cond-mat/0501738* (unpublished) and the experimental refs. [23-26] therein.
- ²³ Y. Tokura, H. Kuwahara, Y. Moritomo, Y. Tomioka, and A. Asamitsu, *Phys. Rev. Lett.* **76**, 3184 (1996).
- ²⁴ Y. Tokura, and Y. Tomioka, *J. Magn. Magn. Mater.* **200**, 1 (1999).
- ²⁵ A. Biswas, A. Arulraj, A. K. Raychaudhuri, and C. N. R. Rao, *J. Phys. Cond. Matt* **12** L101 (2000).
- ²⁶ S. K. Mishra, R. Pandit, and S. Satpathy, *Phys. Rev. B* **56**, 2316 (1997).
- ²⁷ S. Fratini, D. Feinberg, and M. Grilli, *Eur. Phys. J. B* **22**, 157 (2001).
- ²⁸ J van den Brink, G. Khaliullin, and D. Khomskii, *Phys. Rev. Lett.* **83**, 5118 (1999).
- ²⁹ G. Jackeli, N. B. Perkins, and N. M. Plakida, *Phys. Rev. B* **62**, 372 (2000).
- ³⁰ Z. Shu, J. Dong, D. Y. Xing, *Phys. Rev. B* **63**, 224409 (2001).
- ³¹ T. Hotta, A.-L. Malvezzi, E. Dagotto, *Phys. Rev. B* **62**, 9432 (2000); S. Yunoki, T. Hotta, E. Dagotto, *Phys. Rev. Lett.* **84**, 3714 (2000); for an extensive discussion of related numerical work, see also the review by Dagotto *et al.* in Ref. [1].
- ³² H. Aliaga, D. Magnoux, A. Moreo, D. Poilblanc, S. Yunoki, and E. Dagotto, *Phys. Rev. B* **68**, 104405 (2003).
- ³³ T. V. Ramakrishnan, H. R. Krishnamurthy, S. R. Hassan, and G. Venketeswara Pai, *Phys. Rev. Lett.* **92**, 157203 (2004); for a more detailed discussion, see Ramakrishnan T. V., Krishnamurthy H. R., Hassan S. R. and Venketeswara Pai G. 2003, in *Colossal Magnetoresistive Manganites*, ed. Chatterji T., (Kluwer Academic Publishers, Dordrecht, Netherlands, 2004), *cond-mat/0308396*.
- ³⁴ The CE phase, in particular, breaks the translation invariance of the reference cubic Mn lattice so as to generate a unit cell with eight inequivalent sites.
- ³⁵ P.-G. de Gennes, *Phys. Rev.* **118**, 141 (1960).
- ³⁶ M. Roy, J. F. Mitchell, A. P. Ramirez, P. Schiffer, *Phys. Rev. B* **58**, 5185 (1998).
- ³⁷ G. C. Milward, M. J. Calderon and P. B. Littlewood, *Nature* **433**, 607 (2005).
- ³⁸ T. A. Tyson, M. Deleon, M. Croft, V. G. Harris, C.-C. Kao, J. Kirkland, and S.-W. Cheong, *Phys. Rev. B* **70**, 024410 (2004).
- ³⁹ H. Nojiri, private communication.
- ⁴⁰ O. Cépas, H. R. Krishnamurthy, and T. V. Ramakrishnan, *Phys. Rev. Lett.* **94**, 247207 (2005).
- ⁴¹ The e_g atomic orbitals of Mn and the appropriate p_σ atomic orbitals of O are known to hybridize very strongly. We assume that the bonding bands made-up of Wannier orbitals predominantly of $O - p_\sigma$ character are fully occupied, and are "projected out" so that the projected "effective Hamiltonian" can be written using Wannier orbitals with e_g symmetry as we have done. We emphasize that these orbitals are not to be regarded pure Mn orbitals, but include components that are the appropriate, symmetry determined combinations of the surrounding O orbitals as well. But their specific composition involves band structure details that we have not included in our considerations. However, issues of considerable current interest, such as the distribution of the charge on the Mn and O ions in the CE and other phases,^{9,10,11,17} would be governed by the precise composition of the Wannier orbital, and could interpolate between the various conflicting pictures of the charge and orbital order depending on the band-structure details.
- ⁴² P. W. Anderson and H. Hasegawa, *Phys. Rev.* **100**, 675 (1955).
- ⁴³ While this projection for the $J_H \rightarrow \infty$ limit obtained by approximating the t_{2g} spins as classical is widely used, an approach valid for quantum t_{2g} spins using a representation in which the total spin ($\vec{S}_i + \vec{S}_i$) is diagonal is discussed in the review article by Loktev and Pogorelov [2].
- ⁴⁴ A compact way of writing the hopping matrix elements in the form of an outer product of orbital pseudo-spinor wavefunctions:
- $$t_{abij}^{\alpha\beta} = (4t/3)\zeta_{abij}^\alpha\zeta_{abij}^\beta$$
- The pseudo-spinors corresponding to hopping in the 3 cubic directions are,
- $$\zeta_x = (\sqrt{3}/2, -1/2); \zeta_y = (-\sqrt{3}/2, -1/2); \zeta_z = (0, 1).$$
- ⁴⁵ eg., see A. J. Millis, *Phys. Rev. B*, **55**, 6405 (1997).
- ⁴⁶ A. J. Millis, *Phys. Rev. B*, **53**, 8434 (1996).
- ⁴⁷ N. Furukawa, *cond-mat/9812066*; see also the extensive numerical work by Dagotto and co-workers discussed in their review cited in Ref. [1] and references therein, and the recent work of S. Kumar and P. Majumdar, *Phys. Rev. Lett.* **91**, 246602 (2003).

- ⁴⁸ Note that the difference between the critical values of $J_{AF}S^2/t$ at $g = 0$ with that of Refs. [28,29] with $V = 0$ comes from a different definition of t by a factor $4/3$ but the results perfectly agree otherwise.
- ⁴⁹ In writing this, we have neglected terms proportional to $n_i n_j$ since, as we have seen, for the half doped case and for large g/t there is nearly complete charge disproportionation, whence they are smaller by a factor of t/E_{JT} compared to the term retained above even when U is zero, and are completely suppressed for large U .
- ⁵⁰ S. Ishihara, J. Inoue, and S. Maekawa, Phys. Rev. B **55**, 8280 (1997).
- ⁵¹ S.-Q. Shen, Phys. Rev. Lett. **86**, 5842 (2001).
- ⁵² I. V. Soloviyev and K. Terakura, Phys. Rev. Lett. **83**, 2825 (1999).
- ⁵³ We note that it would be important to take into account the cooperative nature of the distortions if one wants to give a quantitative account of the energies. This would in particular modify the distortions of the corner sites. Since we are using the simpler framework of non-cooperative JT phonons, we therefore neglect the small distortions of the corner sites also at this stage.
- ⁵⁴ Z. Popovic and S. Satpathy, Phys. Rev. Lett. **88**, 197201 (2002).
- ⁵⁵ B. P. Sekhar, S. Kumar, and P. Majumdar, Europhys. Lett. **68**, 564 (2004).
- ⁵⁶ M. Yu. Kagan, D. I. Khomskii, and M. V. Mostovoy, Eur. Phys. J. B **12**, 217 (1999).
- ⁵⁷ H. Meskine, T. Saha-Dasgupta, and S. Satpathy, Phys. Rev. Lett. **92**, 056401 (2004).
- ⁵⁸ The transition line between the CE-M-C and the CE-T phases vanishes at $x = 1/2$, as seen in the figure, because the conduction band in the CE phase is dispersionless in the nearest neighbor model we have considered. With a more realistic model, the transition would occur at a finite g/t at $x = 1/2$.
- ⁵⁹ We can fit the resistivity-temperature curve to get an estimation of the gap. We find a gap of the order of 500 K from Ref. [8], which is much smaller than t .
- ⁶⁰ Finite temperature results for the phase diagram at zero-field and half-doping have been recently reported in L. Brey, Phys. Rev. B **71**, 174426 (2005). As far as zero temperature results are concerned, they agree with that of Ref. [40] and the present work.
- ⁶¹ Recently, Brey and Littlewood have proposed that 'orbital solitons' occur upon doping the CE phase, and that the particle-hole asymmetry is due to the energy difference between positive and negative energy solitons [L. Brey, and P. B. Littlewood, Phys. Rev. Lett. **95**, 117205 (2005)]. These defects are different from the ones considered by us in that their appearance involves a complete and large-scale rearrangement of the magnetic order of the CE phase.
- ⁶² A. Georges, G. Kotliar, W. Krauth, and M. Rozenberg, Rev. Mod. Phys. **68** 13 (1996).